เทคโนโลยีที่เป็นมิตรกับสิ่งแวดล้อมสำหรับการกำจัดตะกั่วจากน้ำเสียแบตเตอรี ด้วยการดัดแปรลิ้นทะเลเป็นวัสดุดูดซับทางชีวภาพ

นายปฐมพงศ์ วิภาตะพันธุ์

วิทยานิพนธ์นี้เป็นส่วนหนึ่งของการศึกษาตามหลักสูตรปริญญาวิทยาศาสตรมหาบัณฑิต
สาขาวิชาเทคโนโลยีชีวภาพ
คณะวิทยาศาสตร์ จุฬาลงกรณ์มหาวิทยาลัย
ปีการศึกษา 2558

ENVIRONMENTAL FRIENDLY TECHNOLOGY FOR REMOVAL OF LEAD FROM BATTERY WASTEWATER USING MODIFICATION OF CUTTLEBONE AS BIOSORBENT

Mr. Pathompong Vibhatabandhu

A Thesis Submitted in Partial Fulfillment of the Requirements
for the Degree of Master of Science Program in Biotechnology
Faculty of Science
Chulalongkorn University
Academic Year 2015

Thesis Title	ENVIRONMENTAL FRIENDLY TECHNOLOGY FOR REMOVAL OF LEAD FROM BATTERY WASTEWATER USING MODIFICATION OF CUTTLEBONE AS BIOSORBENT
By	Mr. Pathompong Vibhatabandhu
Field of Study	Biotechnology
Thesis Advisor	Sarawut Srithongouthai, Ph.D.

Accepted by the Faculty of Science, Chulalongkorn University in Partial Fulfillment of the Requirements for the Master's Degree

.....Dean of the Faculty of Science
(Associate Professor Polkit Sangvanich, Ph.D.)

THESIS COMMITTEE

.....Chairman
(Sitthichok Puangthngthub, Ph.D.)

.....Thesis Advisor
(Sarawut Srithongouthai, Ph.D.)

.....Examiner
(Associate Professor Sirilux Poompradub, Ph.D.)

.....External Examiner
(Marut Suksomjit, Ph.D.)

ปฐมพงศ์ วิภาตะพันธุ์ : เทคโนโลยีที่เป็นมิตรกับสิ่งแวดล้อมสำหรับการกำจัดตะกั่วจากน้ำเสียแบตเตอรีด้วยการดัดแปรลิ้นทะเลเป็นวัสดุดูดซับทางชีวภาพ (ENVIRONMENTAL FRIENDLY TECHNOLOGY FOR REMOVAL OF LEAD FROM BATTERY WASTEWATER USING MODIFICATION OF CUTTLEBONE AS BIOSORBENT) อ.ที่ปรึกษาวิทยานิพนธ์หลัก: อ. ดร. สราวุธ ศรีทองอุทัย, หน้า.

การศึกษาครั้งนี้เป็นการศึกษาเพื่อสร้างนวัตกรรมวัสดุดูดซับทางชีวภาพที่เป็นมิตรต่อสิ่งแวดล้อมเพื่อกำจัดตะกั่วออกจากน้ำเสียในกระบวนการผลิตแบตเตอรี ดังนั้น พฤติกรรมในการดูดซับตะกั่วด้วยลิ้นทะเลจึงถูกวิเคราะห์เพื่อประยุกต์ใช้ในการกำจัดน้ำเสียจากกระบวนการผลิตแบตเตอรี ซึ่งการศึกษาครั้งนี้แสดงให้เห็นว่าการดัดแปรลิ้นทะเลสามารถประยุกต์ใช้เป็นวัสดุดูดซับทางชีวภาพสำหรับกำจัดโลหะหนักออกจากน้ำเสียได้อย่างมีประสิทธิภาพ โดยทำการศึกษาศักยภาพการกำจัดตะกั่วจากน้ำเสียสังเคราะห์และน้ำเสียจากกระบวนการผลิตแบตเตอรีด้วยผงลิ้นทะเล (CB-P) และลิ้นทะเลดัดแปรด้วยการคาร์บอไนเซชันที่อุณหภูมิ 400 องศาเซลเซียส (CB-M400) ด้วยการทดลองแบบกะ ผลการศึกษาแสดงให้เห็นว่า แคลเซียมคาร์บอเนตซึ่งเป็นองค์ประกอบหลักของ CB-P และ CB-M400 เป็นปัจจัยที่ส่งผลต่อการกำจัดตะกั่ว ด้วยการเกิดสารประกอบคาร์บอเนตบนผิวของวัสดุดูดซับ สำหรับการกำจัดตะกั่ว ด้วยวัสดุดูดซับทั้งสองชนิดมีประสิทธิภาพสูงสุดในภาวะของสารละลายที่มีความเป็นกรด-ด่างเท่ากับ 4.0 และใช้วัสดุดูดซับปริมาณ 0.2 กรัมต่อลิตร จากการศึกษาสมดุลการดูดซับแสดงให้เห็นว่าไอโซเทอร์มของแลงเมียร์สามารถอธิบายการดูดซับตะกั่วบนวัสดุดูดซับโดยมีค่าสัมประสิทธิ์สหสัมพันธ์สูง (R^2>0.9329) ความสามารถในการดูดซับตะกั่วสูงสุดซึ่งคำนวณจากไอโซเทอร์มมีค่า 869.57 มิลลิกรัมต่อกรัม สำหรับ CB-P และ 1573.56 มิลลิกรัมต่อกรัม สำหรับ CB-M400 ในการศึกษาจลนศาสตร์การดูดซับพบว่า การดูดซับตะกั่วเข้าสู่สมดุลภายในเวลา 240 นาที และสอดคล้องกับแบบจำลองปฏิกิริยาอันดับสองเทียม จากการศึกษาการกำจัดตะกั่วจากน้ำเสียแบตเตอรีพบว่า เหล็ก และโครเมียมไอออน ที่ปนเปื้อนในน้ำเสียมีการรบกวนกระบวนการดูดซับตะกั่ว นอกจากนั้น ผลการทดลองสามารถประยุกต์การบำบัดขั้นต้นด้วยแคลเซียมไฮดรอกไซด์ร่วมกับวัสดุดูดซับเพื่อการกำจัดตะกั่วจากน้ำเสียจากการผลิตแบตเตอรีได้อย่างมีประสิทธิภาพ

สาขาวิชา เทคโนโลยีชีวภาพ ลายมือชื่อนิสิต .....

ปีการศึกษา 2558 ลายมือชื่อ อ.ที่ปรึกษาหลัก .....

5772038823 : MAJOR BIOTECHNOLOGY
KEYWORDS: LEAD REMOVAL / BIOSORBENT / CUTTLEBONE / BATTERY WASTEWATER

PATHOMPONG VIBHATABANDHU: ENVIRONMENTAL FRIENDLY TECHNOLOGY FOR REMOVAL OF LEAD FROM BATTERY WASTEWATER USING MODIFICATION OF CUTTLEBONE AS BIOSORBENT. ADVISOR: SARAWUT SRITHONGOUTHAI, Ph.D., pp.

The present study, the innovative biosorbent for treating acid battery manufacturing wastewater containing Pb (II) was studied in order to meet eco-friendly technology. Therefore, the Pb(II) adsorption behavior of cuttlebone was analyzed its applicability in treating acid battery manufacturing wastewater. This study showed that, the modification of cuttlebone can be applied to effective biosorbent for heavy metals removal from wastewater. Ability of cuttlebone powder (CB-P) and cuttlebone modified by carbonization at 400 °C (CB-M400) for removal of Pb (II) from Pb (II) synthetic and battery wastewater are carried out using a batch adsorption system. The results showed that mainly consisted $CaCO_3$ in CB-P and CB-M400 was affected to Pb (II) removal by CO_3^{2-} complexation on adsorbent surface. The Pb (II) removal of both adsorbents was recorded optimum performance in solution pH 4.0 with adsorbent dose of 0.2 g/L. According to the adsorption equilibrium study, the very high correlation coefficients (R^2>0.9329) of Langmiur isotherm can used to explain Pb adsorption in both adsorbents. The maximum Pb adsorption capacity that calculated from isotherm was 869.57 mg/g for CB-P and 1573.56 mg/g for CB-M400. In adsorption kinetic study, biosorption rate was fast and most of the process was completed within 240 minutes, according to the pseudo-second order model. In addition, Pb adsorption was interfered by competitive adsorption of contaminated Fe (II) and Cr (III) in battery wastewater. However, combination of $Ca(OH)_2$ pretreatment following adsorbents addition was efficiently removed lead from acid battery manufacturing wastewater.

Field of Study: Biotechnology Student's Signature .....

Academic Year: 2015 Advisor's Signature .....

ACKNOWLEDGEMENTS

I am very proud to say that this thesis was completed with the valuable advice, continuous guidance, constructive criticism and encouragement of my adviser, Sarawut Srithongouthai, Ph. D., throughout the course of my study. His kindness and generosity will always be remembered.

I am deeply gratitude to the members of my thesis committee, Sitthichok Puangthongthub, Ph. D., Associate Professor Sirilux Poompradub, Ph. D., Marut Suksumjit, Ph. D. for their valuable comments and suggestions in the completion of this thesis.

Special thanks are gratefully expressed to Ketsaraporn Kaenkaew, member of Department of Environmental Science, Scientific and Technological Research Equipment Centre, Analytical and Testing Service Center of the Petroleum and Petrochemical College and Department of Material Science, Chulalongkorn University for laboratory supports and analytical services.

I also extended acknowledges to Program in Biotechnology, Faculty of Science, Chulalongkorn University and Graduate School of Chulalongkorn University

Finally, I would like to thanks the others and my parents for their support, encouragement and understanding throughout graduate study.

CONTENTS

Page
THAI ABSTRACT iv
ENGLISH ABSTRACT v
ACKNOWLEDGEMENTS vi
CONTENTS vii
CHAPTER I INTRODUCTION 1
1.1 Statement of the problem 1
1.2 Objectives 2
1.3 Scope of the research 3
CHAPTER II THEORY AND LITERATURE REVIEW 5
2.1 The chemistry of lead in an aqueous system 5
2.1.1 Speciation of dissolution 5
2.1.2 Precipitation 7
2.2 Oxidation-reduction 9
2.3 Adsorption 10
2.3.1 Biosorption 10
2.3.2 Adsorption equilibrium 10
2.3.3 Adsorption kinetic 13
2.4 Cuttlebone 14
2.5 Lead-acid battery wastewater 15
2.6 Literature review 17
CHAPTER III EXPERIMENTALS 20
3.1 Chemicals 20
3.2 Instruments 21
3.3 Experimental method 22
3.3.1 Preparation of adsorbent 22
3.3.2 Physicochemical characteristic of adsorbent 22
3.3.3 Adsorption experiment 23
3.3.4 Effect of controlling factors on Pb (II) adsorption 24

Page

3.3.5 Adsorption kinetic 26
3.3.6 Adsorption interference 27
3.3.7 Battery wastewater treatment procedures 27
3.3.8 Data analysis 27
CHAPTER IV RESULTS AND DISCUSSION 29
4.1 Physicochemical characteristics of adsorbent 29
4.1.1 Functional group 29
4.1.2 Surface structure 31
4.2 Effect of controlling factors on lead removal 37
4.2.1 Effect of initial pH 37
4.2.2 Effect of adsorbent dose and Pb (II) initial concentration 41
4.3 Adsorption isotherms 43
4.4 Adsorption kinetic 45
4.5 Adsorption interference 48
4.6 Battery wastewater 50
4.6.1 Wastewater composition 50
4.6.2 Wastewater treatment procedure 50
CHAPTER V CONCLUSION AND FUTURE RESEARCH 60
5.1 Conclusion 60
5.2 Future research 61
REFERENCES 62
APPENDIX 67
APPENDIX A 68
APPENDIX B 73
APPENDIX C 75
APPENDIX D 78
APPENDIX E 80
APPENDIX F 82
VITA 89

LIST OF TABLES

TABLE		Page
2.1	Stability constants of Pb-ligand complexes	6
2.2	Solubility product (K_{sp}) of solid complexes	8
2.3	Half-reactions and the redox potential (E^0) [3, 4]	9
3.1	List of chemicals used in present study	20
3.2	List of instruments used in present study	21
3.3	Battery wastewater treatments	27
3.4	Wastewater quality parameters measurement	28
4.1	Mineral content and extracted content of adsorbents	30
4.2	Surface analysis using surface area analyzer	34
4.3	Elements on adsorbents' surfaces before and after adsorption of Pb (II) by SEM-EDS	34
4.4	Quantitative analysis of crystalline in CB-P and CB-M400	35
4.5	Adsorption isotherm parameters	44
4.6	Comparison of maximum Pb (II) adsorption capacity	44
4.7	Adsorption kinetic model parameters	46
4.8	Battery wastewater quality parameters with measured values and industrial effluent standard limits	51
B-1	One-way ANOVA of capacity and efficiency between group CB-P and CB-M400 in effect of initial pH study	73
B-2	Pb (II) adsorption capacity and efficiency of CB-P and CB-M400 in effect of initial pH study with statistic significant between pH	74
C-1	One-way ANOVA of capacity and efficiency between group CB-P and CB-M400 in effect of adsorbent dose and Pb (II) initial concentration study	75
C-2	One-way ANOVA of capacity and efficiency in each concentration between group CB-P (a) and CB-M400 (b)	76

TABLE Page

C-3 Pb (II) adsorption capacity and efficiency of adsorbent dose of CB-P (a) and CB-M400 (b) with statistic significant between adsorbent doses in each concentration 77

D-1 One-way ANOVA of capacity between group CB-P and CB-M400 in kinetic study 78

D-2 Pb (II) adsorption capacity (mg/g) of CB-P and CB-M400 in kinetic study with statistic significant between contact times 79

E-1 One-way ANOVA of Pb adsorption capacity between group CB-P and CB-M400 in single Pb, Pb+Cr and Pb+Fe system 80

E-2 Pb (II) adsorption capacity (mmol/g) of CB-P and CB-M400 in interference study with statistic significant between contact times of single Pb, Pb + Cr and Pb + Fe system 81

F-1 Wastewater quality and composition measurement procedure 82

F-2 One-way ANOVA of wastewater quality after processed treatment I between group CB-P and CB-M400 83

F-3 Data of wastewater quality after process treatment I with statistic significant between doses 84

F-4 One-way ANOVA of wastewater quality after processed treatment II between group CB-P and CB-M400 85

F-5 Data of wastewater quality after process treatment II with statistic significant between doses 86

F-6 One-way ANOVA of wastewater quality after processed treatment III between group CB-P, CB-M400, CaCO3 and Ca(OH)2 87

F-7 Data of wastewater quality after process treatment III with statistic significant between doses 88

LIST OF FIGURES

FIGURE Page

2.1 Predominant area diagram for system $Pb^{2+}/SO_4^{2-}/OH^-$ 6

2.2 The log Concentration-pH for total dissolved Pb in equilibrium with $Pb(OH)_{2(s)}$, $PbCO_{3(s)}$, and $PbSO_{4(s)}$ 8

2.3 Schematic diagrams of cuttlebone position (a) and its transverse section (b) ... 15

2.4 Flow diagram of the lead-acid battery manufacturing process 16

2.5 Schematic diagram of lead-acid battery wastewater treatment plant 16

4.1 FITR spectra of CB-P (a), CB-M400 (b), extracted contents from CB-P (c), and extracted contents from CB-M400 (d) 30

4.2 Surface structures of CB-P and CB-M400 before Pb (II) adsorption, at a magnification of 3,500x (a) and 10,000x (b) by SEM-EDS 32

4.3 Surface structures of CB-P and CB-M400 after Pb (II) adsorption* at a magnification of 1,000x (a) and 3,500x (b) by SEM-EDS 33

4.4 XRD patterns of $CaCO_3$ aragonite (⬢), $CaCO_3$ calcite (△), $PbCO_3$ (○), and $Pb_3(CO_3)_2(OH)_2$ (★) in CB-P and CB-M400, before (a) and after Pb (II) adsorption (b) 35

4.5 Percentage of particulate adsorbent (■) and dissolved matter (□) of CB-P (a) and CB-M400 (b) in aqueous solution at a pH of 1.0-5.0 and distilled water (DW) 38

4.6 Effect of initial pH on Pb (II) adsorption capacity (a) and efficiency (b) in CB-P (◆) and CB-M400 (□) 38

4.7 Altered pH (ΔpH) of synthetic wastewater after Pb (II) adsorption by CB-P (◆) and CB-M400 (□) 39

4.8 Effect of adsorbents dosage and Pb (II) initial concentration in adsorption capacity (a) and adsorption efficiency (b) of CB-P and CB-M400 42

4.9 Adsorption capacities of CB-P (a) and CB-M400 (b) from 5-360 minutes .. 46

4.10 Intra-particle diffusion kinetics of Pb (II) onto CB-P and CB-M400, with initial concentrations of 100 mg/L (a) and 500 mg/L (b) 47

FIGURE Page

4.11 Pb (II) adsorption capacity of CB-P (a) and CB-M400 (b) in single Pb (II) system (●), Pb (II) + Fe (II) system (□), and Pb (II) + Cr (III) system (▲).....48

4.12 Industrial effluent standard limits (▪▪▪▪) and wastewater quality parameters (pH, TDS, Pb, Cr, Ni, Zn, Mn, and Fe) after processing using treatment I with CB-P (◆) and CB-M400 (□).....53

4.13 Concentration of heavy metals in dissolved battery wastewater with pH of 4.0 (adjusted by NaOH).....54

4.14 Industrial effluent standard limits (▪▪▪▪) and wastewater quality parameters (pH, TDS, Pb, Cr, Ni, Zn, Mn, and Fe) after processing using treatment II with CB-P (◆) and CB-M400 (□) 55

4.15 Industrial effluent standard limits (▪▪▪▪) and wastewater quality parameters (pH, TDS, Pb, Cr, Ni, Zn, Mn, and Fe) after processing using treatment III with CB-P (◆), CB-M400 (□), $CaCO_3$ (●), and $Ca(OH)_2$ (△) .57

A-1 XRD pattern of CB-P before Pb adsorption 69

A-2 XRD pattern of CB-M400 before Pb adsorption 70

A-3 XRD pattern of CB-P after Pb adsorption 71

A-4 CB-M400 after Pb adsorption.....72

CHAPTER I
INTRODUCTION

1.1 Statement of the problem

Expanding populations, along with concomitantly increased industrial operations and energy consumption, as well as new industries based upon novel technology, have intensified environmental problems in the areas of water supply, waste disposal, air pollution, toxic contamination, and global climate change. The contamination of heavy metals has become a serious issue due to their toxicity accumulation and magnification in the ecological food chain, which poses an increased risk to human health. Among the various sources of this problem, anthropogenic industrial wastewater is the one that causes the most contamination.

The contamination of Pb and other heavy metals in lead-acid battery effluent is considered a wastewater treatment issue because the latter's quality (Table 4.7) is over the standard limit. To be specific, it has an extremely low pH and a concentration of totally dissolved solids, and is contaminated with Pb, which is known as a highly toxic heavy metal that causes poisoning in the kidney, liver, brain, and nervous system. To address this, various technologies in wastewater treatment have been developed to contain the quality of industrial effluents within a specified standard limit before discharging them to the environment. These techniques include chemical precipitation, coagulation-flocculation, flotation, membrane filtration, ion-exchange, and adsorption, which are all aimed at the removal of Pb and other heavy metals [1, 2].

Chemical precipitation is one of the most widely used methods in this area. In the precipitation process, the reaction of heavy metal ions and ligand ions, including hydroxide, sulfide, and chelating reagents, forms insoluble metal complexes that are ineffective in removing low concentration of metal ions from wastewater and generate large amounts of high-water-content sludge. A more promising approach is adsorption, which is proposed as an economical and effective method for the retention of heavy metal ions from aqueous industrial wastes. As its efficiency depends on the type of adsorbents, many varieties of the latter have been developed and tested [1, 2].

To reduce waste generation, the use of biomass waste or byproducts has been studied and investigated in heavy metals removal through a biosorption process. Cuttlebone is a waste product from the harvesting of cuttlefish for food, and is commonly used as a traditional medicine or, to a lesser extent, a calcium-rich dietary supplement. Due to its lower level of utilization, in this research interested in the modification of cuttlebone to be applied as a biosorbent for the removal of Pb (II) from aqueous solution. In preliminary tests of the use of 2 g/L of cuttlebone powder to adsorb Pb (II) at a concentration of 500 mg/L, with pH of 3.0, in a fixed time of 240 minutes and at a shake speed of 100 rpm, a high efficiency of Pb removal (99.45 ± 0.95 %) was expressed. In order to improve the efficacy of biosorbents, this study focuses on evaluating the potential of modified cuttlebone adsorbents to remove Pb (II) from aqueous solution, with a view to applying them in battery wastewater treatment.

1.2 Objectives

1.2.1 To assess the controlling factors of Pb (II) adsorption capacity and efficiency in modified cuttlebone biosorbents.

1.2.2 To explain the Pb (II) adsorption equilibrium and the kinetic of biosorbents.

1.2.3 To characterize the chemical composition of battery wastewater and study the interference of Pb (II) adsorption.

1.2.4 To apply modified cuttlebone in battery wastewater treatment.

1.3 Scope of the research

1.3.1 Reviewing of relevant previously published research.

1.3.2 Design and preparation of the experimental procedure and chemicals.

1.3.3 Preparation of adsorbents from cuttlebone, as follows:

1) Cuttlebone powder (CB-P)

2) Cuttlebone modified by carbonization at 400 °C (CB-M400)

1.3.4 Studying of the physicochemical properties of cuttlebone:

1) Adsorbents and contents, as extracted by 1 M HCl at ambient temperature for three hours with HCl: adsorbent ratio of 40 mL/g, are characterized into functional groups.

2) Measuring surfaces of adsorbents, including specific surface area, total pore volume, pore size, structure, element, and crystalline chemical of adsorbents.

1.3.5 Removal of Pb (II) from aqueous solution and process it using a batch system.

1.3.6 Calculating of the take-up capacity and efficiency of Pb (II).

1.3.7 Assessing of the effect of controlling factors, including initial pH, initial concentration of Pb (II), and adsorbents dosage, by experimenting with $Pb(NO_3)_2$ synthetic wastewater in a fixed time of 240 minutes at a shake speed of 100 rpm and a temperature of 30 °C.

1.3.8 Analyzing of Pb (II) adsorption isotherm via the linear form of Langmuir isotherm and Freundlich isotherm.

1.3.9 Studying of Pb (II) adsorption's kinetic using the following method:

1) Analyze dissolved Pb concentration in sampling solution at different times while assuming that the initial concentration is equal for all durations.

2) Determine the reaction rate using pseudo-first-order and pseudo-second-order kinetic models.

1.3.10 Studying of the effect of interference ions on Pb (II) adsorption while combining binary heavy metals and synthetic wastewater in Pb (II) and Fe (II) systems and Pb (II) and Cr (III) systems.

1.3.11 Applying of modified cuttlebone to lead-acid battery wastewater treatment to assess wastewater pH; to compare total dissolved solid and heavy metals (Pb, Cr, Ni, Zn, Mn, and Fe) of dissolved wastewater with $CaCO_3$ and $Ca(OH)_2$.

1.3.12 Analyzing of data, summarize the results, and write thesis.

CHAPTER II
THEORY AND LITERATURE REVIEW

2.1 The chemistry of lead in an aqueous system

2.1.1 Speciation of dissolution

Water molecules with negative charge are weakly bonded, with unshared electrons, to Pb ions, also known as free or uncomplex Pb ions. A variety of other molecules, such as OH^-, Cl^-, F^-, NH_3, and SO_4^{2-}, which can replace the water molecules surrounding the metal, are referred to as ligands; an entire molecule is called a metal-ligand complex or simply a complex. A Pb complex with OH^- is illustrated via the following reaction:

$$Pb^{2+} + OH^- \leftrightarrow PbOH^+ \qquad K_1 \qquad (2.1)$$

$$PbOH^+ + OH^- \leftrightarrow Pb(OH)_2 \qquad K_2 \qquad (2.2)$$

$$Pb(OH)_2 + OH^- \leftrightarrow Pb(OH)_3^- \qquad K_3 \qquad (2.3)$$

$$Pb(OH)_3^- + OH^- \leftrightarrow Pb(OH)_4^{2-} \qquad K_4 \qquad (2.4)$$

The attraction of electron pairs on water molecules to metal ions cause H^+ ions in a part of the water molecule to dissociate more easily, with the result that the metal ions act as an acid. The net effect is that they are replaced by OH^- ions as one of the ligands in the reaction. The stability constants, formation constants, or equilibrium constants (K) of the forming metal-ligand complex reaction are listed in Table 2.1. Varying amounts of ligands can form complexes with certain metal ions; the $Pb^{2+}/SO_4^{2-}/OH^+$ dominant species of dissolved metal concentrations in variable solutions of pH can correspond with each other in the predominant area diagram (Figure 2.1) [3].

Table 2.1 Stability constants of Pb-ligand complexes [3]

Pb-L complex	Stability constants (log K)							
	OH^-	CO_3^{2-}	SO_4^{2-}	Cl^-	F^-	EDTA	CN^-	HS^-
PbL	6.29	7.24	2.75	1.6	1.25	17.86	-	15.27
PbL_2	4.59	3.4	0.72	0.2	1.31	-	-	1.3
PbL_3	3.06	-	-	0.1	0.86	-	-	-
PbL_4	2.36	-	-	-0.32	-0.32	-	10.6	-
PbHL	-	13.2	-	-	-	9.68	-	-
PbH_2L	-	-	-	-	-	-3.46	-	-

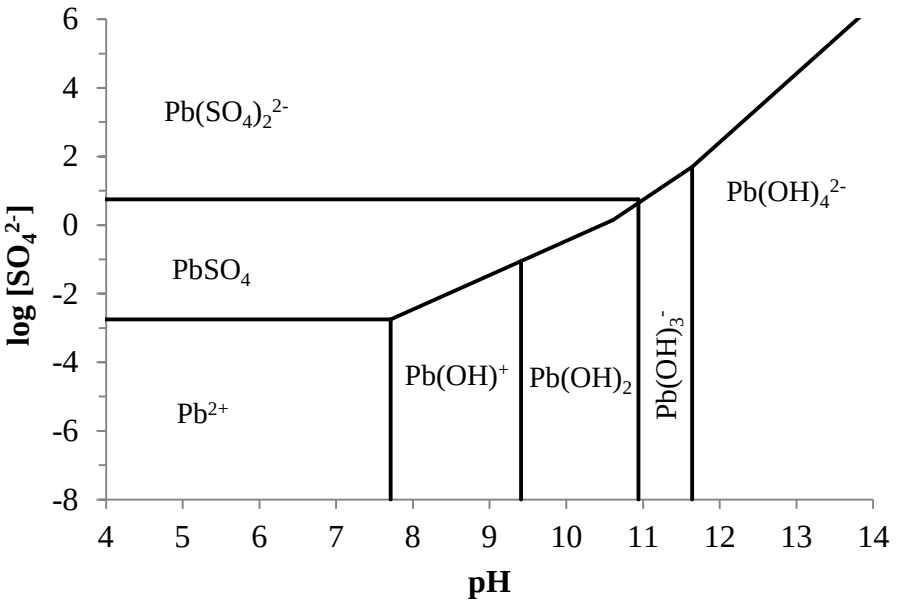

Figure 2.1 Predominant area diagram for system $Pb^{2+}/SO_4^{2-}/OH^-$

2.1.2 Precipitation

Precipitation can be observed in three stages: 1) nucleation, 2) crystal growth, and 3) agglomeration and ripening of the solid. As the concentration of metal and ligand ions in a solution increases slightly to supersaturation, some of the metals start to form larger complexes and become nuclei solids; then, solid crystals are formed and accumulate to larger-sized precipitates. Both dissolved and solid complexes are represented in the system. Considering the Pb/OH system, dissolved Pb and the solid of $Pb(OH)_2$ are expressed through the following equation:

$$Pb(OH)_{2(s)} \leftrightarrow Pb^{2+} + 2OH^{-} \qquad K_{sp} \qquad (2.5)$$

The equilibrium constant or solubility product (K_{sp}) describes the corresponding ratio of dissolved complex and solid in the equilibrium. In a similar way to the formation of soluble complexes, metals can form solids with a variety of ligands; the K_{sp} of Pb solid complexes and some other solid complexes are listed in Table 2.2. The total dissolved Pb (Pb (II) and Pb-ligands complexes) concentration with Pb solid complexes, as shown in Figure 2.2, are related to the solution pH [3, 4].

Table 2.2 Solubility product (K_{sp}) of solid complexes [3, 4]

Solid	Log (K_{sp})	Solid	Log (K_{sp})
$Pb(OH)_2$	-14.3	$Fe(OH)_3$	-37.11
$PbSO_4$	-7.8	$Fe(OH)_2$	-15.9
$PbCO_3$	-13.13	$FeCO_3$	-10.55
$Pb_3(CO_3)_2(OH)_2$	-45.46	$Zn(OH)_2$	-17.2
$CaCO_3$ (Calcite)	-8.48	$ZnCO_3 \cdot H_2O$	10.26
$CaCO_3$ (Aragonite)	-8.36	$Cr(OH)_3$	-33.13
$Ca(OH)_2$	-5.32	$Ni(OH)_2$	-17.2
$CaSO_4$	-4.85	$NiCO_3$	-6.84

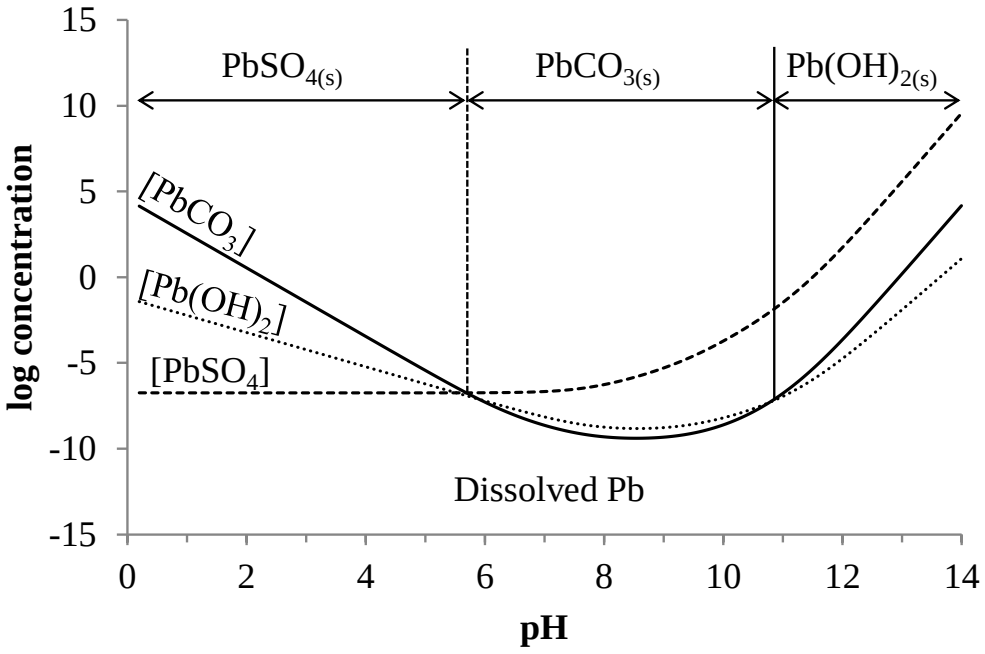

Figure 2.2 The log concentration-pH for total dissolved Pb in equilibrium with $Pb(OH)_{2(s)}$, $PbCO_{3(s)}$, and $PbSO_{4(s)}$*

*Total concentration of CO_3^{2-} and SO_4^{2-} = 0.1 M

2.2 Oxidation-reduction

The oxidation state, or oxidation number of metals and ligands, is dependent upon environmental conditions, such as water pH. Oxidation-reduction or redox reactions, which donate electrons in oxidation and accept them in reduction, play a significant role in the transformation of metals in water. The number of electrons that are reduced and oxidized through an agent in the redox reaction is divided in the half-reaction. At 25 °C, 1 atm, as related to Gibbs free energy (ΔG^0) for the reaction, of redox potential (E^0) can proscribe the direction of the reaction. For positive E^0, the reaction will proceed spontaneously. With an inverse value, in which E^0 is negative, a reverse reaction will occur in an ad-hoc manner [4]. Half-reactions and the standard reduction potential (E^0) as described in this study are listed in Table 2.3.

Table 2.3 Half-reactions and the redox potential (E^0) [3, 4]

Reaction	E^0 (Volt)
$O_{2(aq)} + 4H^+ + 4e^- \leftrightarrow 2H_2O$	+1.27
$PbO_{2(s)} + 4H^+ + SO_4^{2-} + 2e^- \leftrightarrow PbSO_{4(s)} + 2H_2O$	+1.68
$Pb^{2+} + 2e^- \leftrightarrow Pb_{(s)}$	-0.13
$Fe^{2+} + 2e^- \leftrightarrow Fe_{(s)}$	-0.44
$Fe^{3+} + e^- \leftrightarrow Fe^{2+}$	+0.77
$Cr_2O_7^{2-} + 14H^+ + 6e^- \leftrightarrow 2Cr^{3+} + 7H_2O$	+1.33
$CrO_7^{2-} + 3e^- + 8H^+ \leftrightarrow 2Cr^{3+} + 4H_2O$	+1.51
$MnO_{2(s)} + 2e^- + 4H^+ \leftrightarrow Mn^{2+} + 2H_2O$	+1.23
$Mn^{3+} + e^- \leftrightarrow Mn^{2+}$	+1.51
$MnO_4^- + 5e^- + 8H^+ \leftrightarrow Mn^{2+} + 4H_2O$	+1.51
$Ni^{2+} + 2e^- \leftrightarrow Ni_{(s)}$	-0.24
$Zn^{2+} + 2e^- \leftrightarrow Zn_{(s)}$	-0.76

2.3 Adsorption

Adsorption is the accumulation process of adsorbate ions or molecules that tend to concentrate on the surface of solid adsorbents. It is the result of a physical or nonspecific force of attraction or Van der Waal's force, a chemical force that builds a stronger chemical bond for the formation of monolayer compounds on adsorbent surfaces and ion exchanges, in which electrostatic attraction between adsorbate and surface ions has an opposite charge from the binding site [3, 5].

2.3.1 Biosorption

Biosorption, in which pollutants are adsorbed by a non-living biomass, was tested for the removal of heavy metals from contaminated water. Because abundant byproduct biomasses and waste materials are inexpensive and renewable resources, they make highly interesting materials for use in biosorption [6].

2.3.2 Adsorption equilibrium

Described as an adsorption phenomenon, equilibrium is the establishment of a dynamic balance between adsorbates in solution and an adsorbed state in the interface of an adsorbent. A mathematical model, known as an adsorption isotherm, refers to the adsorption equilibrium at constant temperature, which is effectively the relationship between the adsorbed amount per unit of adsorbent or adsorption capacity (q_e) and the remaining adsorbate in the solution (C_e). The most commonly used isotherms are the Langmuir isotherm and the Fruendlich isotherm [7, 8].

1) Langmuir isotherm

The Langmuir isotherm equation can be written as per equation (2.6), but is often written in different linear forms, as per equations (2.7), (2.8), (2.9), and (2.10). Referred to as homogenous adsorption, this isotherm assumes a thickness of the monolayer adsorption which only occurs at a fixed site, given that all sites are similar and have an equal take-up ability as regards the adsorbate [7, 8].

$$q_e = \frac{q_m K_L C_e}{1+K_L C_e} \quad (2.6)$$

$$\frac{C_e}{q_e} = \frac{1}{K_L q_m} + \frac{C_e}{q_m} \quad (2.7)$$

$$\frac{1}{q_e} = \frac{1}{q_m} + \frac{1}{K_L q_m C_e} \quad (2.8)$$

$$q_e = q_m - \frac{q_e}{K_L C_e} \quad (2.9)$$

$$\frac{q_e}{C_e} = K_L q_m - K_L q_e \quad (2.10)$$

Where C_e is the adsorbate concentration at the equilibrium (mg/L)

q_e is the adsorption capacity at the equilibrium (mg/g)

K_L is the Langmuir isotherm constant (L/mg)

q_m is the maximum adsorption capacity (mg/g)

A dimensionless separation factor (R_L), which uses the Langmuir isotherm constant and the initial concentration of the adsorbate (C_i), can be deployed to predict the adsorption affinity, as per equation (2.11).

$$R_L = \frac{1}{1+K_L C_i} \quad (2.11)$$

To explain, a lower R_L value indicates that adsorption is more favorable. For example, the calculated R_L value means that the adsorption characteristic is either unfavorable ($R_L > 1$), linear ($R_L = 1$), favorable ($0 < R_L < 1$), or irreversible ($R_L = 0$) [8, 9].

2) Freundlich isotherm

The Freundlich isotherm model can be applied to the multilayer adsorption of a heterogeneous surface, with non-uniform distribution of adsorption energy and affinities. Equations (2.12) and (2.13) are Freundlich isotherm equations with a non-linear form and a linearized logarithmic form, respectively [7, 8].

$$q_e = K_F C_e^{1/n} \quad (2.12)$$

$$\log q_e = \log K_F + \frac{1}{n} \log C_e \quad (2.13)$$

Where C_e is the adsorbate concentration at the equilibrium (mg/L)

q_e is the adsorption capacity at the equilibrium (mg/g)

K_F is the Freundlich isotherm constant $((mg/g)\cdot(L/g)^n)$

n is the adsorption intensity

2.3.3 Adsorption kinetic

The adsorption reaction model is expressed as the adsorption reaction rate or solute removal rate that controls the residence time of the adsorbate in the solid-solution interface. Adsorption kinetic models have been established to understand the adsorption kinetics and rate-limiting step. The pseudo-first-order and pseudo-second-order rate equations can be expressed as equations (2.14) and (2.15), respectively [7, 10, 11].

$$\frac{dq_t}{dt} = K_1(q_e - q_t) \quad (2.14)$$

$$\frac{dq_t}{dt} = K_2(q_e - q_t)^2 \quad (2.15)$$

Where q_e is the adsorption capacity at the equilibrium (mg/g)

q_t is the adsorption capacity (mg/g) at time t (minute)

K_1 is the pseudo-first-order rate constant (s^{-1})

K_2 is the pseudo-second-order rate constant (g/(mg·minute))

The integration of equations (2.14) and (2.15) gives a linear form equation, as follows:

$$\ln(q_e - q_t) = \ln q_t - K_1 t \quad (2.16)$$

$$\frac{t}{q_t} = \frac{t}{q_e} + \frac{1}{k_2 q_e^2} \quad (2.17)$$

The adsorption diffusion model also identifies the mechanism involved in the adsorption process, through the following three steps: 1) The external mass transfer that is the boundary or film diffusion between the liquid and sorbate film surrounds the adsorbent surface, 2) The internal particular diffusion of mass transportation within the particle-contained pores, and 3) The mass action, or adsorption and desorption, between the adsorbate and active site.

Steps 1) or 2) always control the kinetic process of adsorption; one of them is invariably the rate-limiting step [11, 12]. As represented in equation 2.18, the Weber-Morris model was constructed to describe the process of intra-particle diffusion of heavy metals adsorption [11-15].

$$q_t = K_{int}\sqrt{t} \qquad (2.18)$$

Where q_t is the adsorption capacity (mg/g) at time t (minute)

K_{int} is the intra-particle diffusion rate constant (mg/(g·minute$^{1/2}$))

2.4 Cuttlebone

Cuttlebone, also known as cuttlefish bones or os sepiae, is the internal skeleton of the cuttlefish (*Sepia officinalis*), which gives it buoyancy [16]. About 9 % of a cuttlefish's volume is cuttlebone, which consists of a thick external wall or dorsal shield and an internal lamellar matrix [17]. Schematic diagrams of the cuttlebone's position and its transverse section are shown in Figure 2.3. The parallel sheets or lamellae in the lamellar matrix form numerous calcium carbonate chambers which have corrugated surfaces comprising organic components, whereas the dorsal shell consists of a thick non-porous organic material covering the lamellar matrix [17]. Aragonite crystalline of $CaCO_3$ is a major component of cuttlebone, accounting for 88-97 % of its construction, while the another component is essentially a composite with 1-7 % protein and 3-7 % β-chitin [17-21].

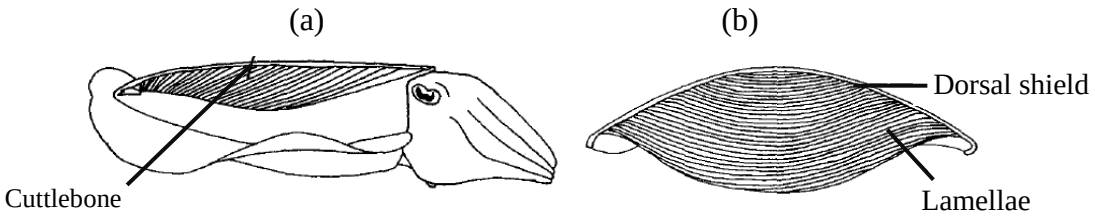

Figure 2.3 Schematic diagrams of cuttlebone position (a) and its transverse section (b) [17]

As they are composed of calcium carbonate, cuttlebones were used in cosmetics, traditional medicine, and animal dietary supplies. Applications of cuttlebone have been researched in chitin-chitosan extraction [18, 19], biomimetic materials [22], and reinforcing filler [21]. Meanwhile, adsorbents, as prepared from cuttlebone, have been investigated for ions adsorption [23-25].

2.5 Lead-acid battery wastewater

Lead-acid batteries are made up of PbO_2 and $PbSO_4$ electrodes and an H_2SO_4 electrolytic solution. A flow diagram of a wet charged battery-manufacturing process is shown in Figure 2.4, which also indicates the areas where lead wastes are generated. In brief, the manufacturing process consists of the application of PbO paste on a lead alloy grid, resulting in the formation of a plate; the plates are then assembled to form a battery, which is charged by filling with sulfuric acid, cooled water, and electric current. Wastewater is generated during the process due to the washing and cleaning of equipment, including the battery plate, as well as during the charging process, while discharging from the scrubber, and in the water-cooling process [26].

Because of the high toxicity of Pb and the standard limit on industrial effluent, wastewater treatment is a necessary process. Lead-acid battery effluent treatment plants (Figure 2.5) were designed to provide a chemical precipitation process. The treatment consists of oil separation, charge neutralization by alum and NaOH addition, precipitation, and sedimentation. In special cases, ion exchange is employed when the total dissolved solid (TDS) is not satisfactory [27].

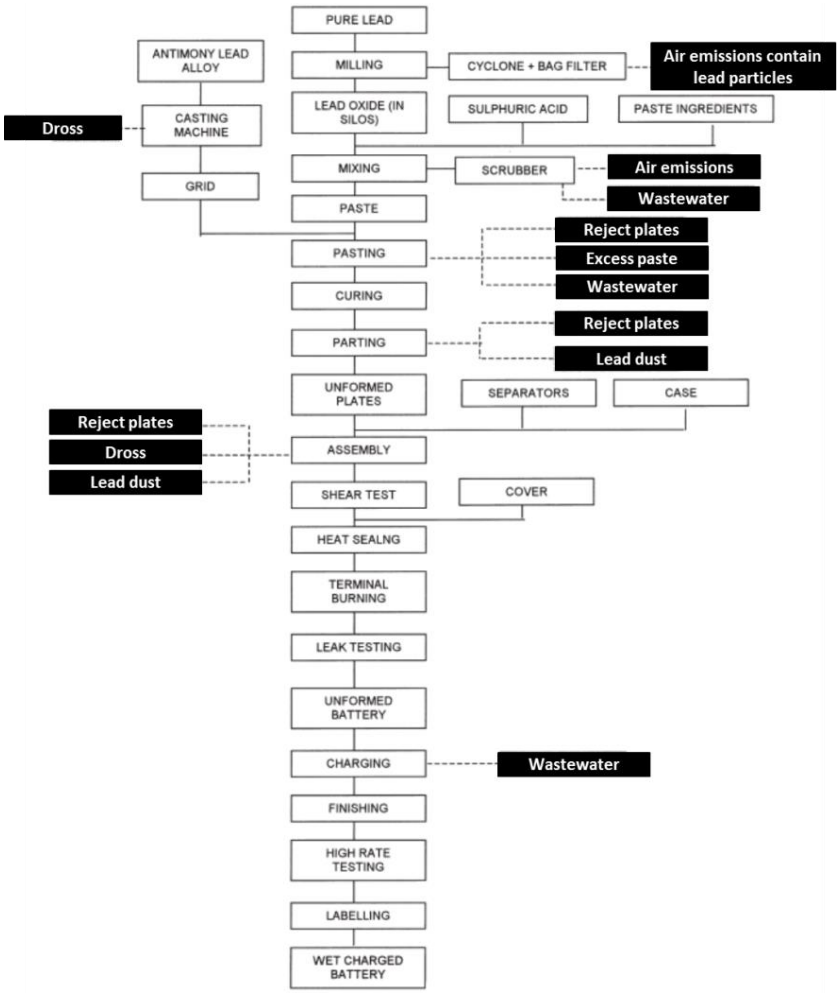

Figure 2.4 **F**low diagram of the lead-acid battery manufacturing process [26]

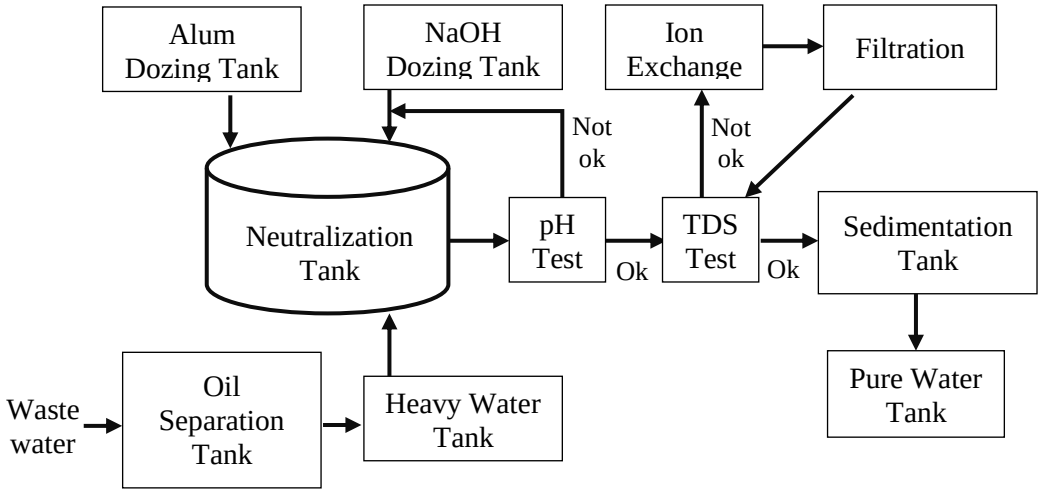

Figure 2.5 Schematic diagram of lead-acid battery wastewater treatment plant [27]

2.6 Literature review

Precipitate solids of $PbCO_3$ and $Pb_3(CO_3)_2(OH)_3$ without $Pb(OH)_2$ and $PbSO_4 \cdot PbO$ are the experimental results of Pb precipitation in the presence of SO_4^{2-} and CO_3^{2-} solution [28]. Accordingly, CO_3^{2-} precipitation is able to treat soluble Pb from battery manufacturing wastewater to lower than 0.2 mg/L [29]. In addition, the synthesized ligand, 1,3-benzenediamido-ethanethiol dianion ($BDET^{2-}$), has seen attention regarding Pb precipitation from battery recycling wastewater. The result was that more than 99.4 % of Pb was removed from an initial concentration of 3.61 mg/L, with predominantly BDET-Pb precipitate, which was stable during 30 day leaching tests [30].

Algae biomasses, including red algae [31], green algae [32], and brown algae [33], have been extensively researched in heavy metals biosorption. Polysaccharide components of the algal cell wall, namely fucoidan and alginic acid or alginate, are functions of metals adsorption. The egg-block structure with a divalent ion of alginate illustrates the accumulated Ca and dissolved heavy metal ion-exchange properties, which are responsible for the affinity with heavy metals uptake [34, 35].

Dehydrated plant biomasses and agricultural waste, such as *Ruppia maritima*, *Echinodorus amazonicus* [36], *Lemna perpusilla* Torr. [37], banana peel[38], peanut shells [39], sawdust [40], and other plant materials with modifications [14, 15, 41, 42] have been studied as heavy metal removal biosorbents. Cellulose, lignin, hemicellulose, extractives, and many compounds found in plant biomasses, mainly contain a variety of functional groups that are present in the heavy metals binding process. Chemisorption, complexation, physisorption on the surface and pores, ion exchange, chelation, and micro-precipitation are involved in heavy metals adsorption mechanisms, as based on adsorbent functional groups [43, 44].

Biochar, which is produced by pyrolysis of plant residue such as hardwood [45], corn straw [45], pecan shells [46], sawdust [46], pinewood [47], rice husks [47], and almond shells [9], has been assessed in terms of heavy metal adsorption. Depending on the pyrolysis process and temperature, the specific surface area and

porosity of biochar have an impact on the adsorption's efficiency. The specific surface area of corn straw biochar, formed by 600 °C slow pyrolysis (13.08 m^2/g), is higher than that of hardwood biochar produced by 450 °C fast pyrolysis (0.43 m^2/g) [45]. With 650 °C pyrolysis, the specific surface area of almond shell biochar is measured as 145 m^2/g [9]. An increasing surface area of pecan shell and sawdust biochar was seen when increasing the pyrolysis temperature from 250-550 °C [46]. However, the higher the temperature, the more the organic matter is degraded by the thermal process [48].

As they contain $CaCO_3$ and natural polysaccharide materials, crab shell [49-52], egg shell [53-56], coral waste [53], and mollusk shell [57] have good potential for heavy metal adsorption. Numerous researchers have pretreated crab shells with HCl and NaOH to eliminate $CaCO_3$ and increase chitin-chitosan biopolymer content for heavy metals adsorption [51, 52, 58]. This is inadvisable, however, as without $CaCO_3$ removal, the heavy metal uptake of crab shell adsorbents is clearly seen to be more effective, because the dissolved $CaCO_3$ content responds to the micro-precipitation properties on the adsorbent surface [49, 58]. Like crab shell, it is possible that other $CaCO_3$ and polysaccharide composite materials can perform the same mechanism. Small-sized eggshell sorbents provide a larger surface area that is available for sorption; in addition, it is easier to dissolve $CaCO_3$compared with the larger particles [54].

Raw cuttlebone 200 mesh adsorbent and NaOH-pretreated cuttlebone adsorbent have been studied with Cu (II) adsorption, with an estimated capacity of 299.26 mg/g in the former and 199.58 mg/g in the latter. NaOH pretreatment involves the deprotonation of adsorbents' surface to express more functional groups and increase the metal adsorption's specific surface area. The metal adsorption mechanism of cuttlebone adsorbent relates to ion exchange, mainly between Ca and metal ions, in terms of even surface complexation, electrostatic adsorption, and micro-deposition. The result also indicated that prepared cuttlebone adsorbents are effective for metal removal from electroplating wastewater [23].

Created micro-pores on the internal surface of cuttlebone have been observed in 0.01 N HCl-treated specimens. A Co (II) adsorption study was conducted on optimized initial concentrations of cobalt (II), pH, sorbent loading, particle size, temperature, and contact time. Kinetic data was fixed with a pseudo-second-order model and adsorption was equilibrated in a time span of 20 minutes. The Langmuir isotherm model fit the experimental data; the maximum capacity of the adsorbent was 76.6 mg/g at 40 °C. The Gibbs free energy (ΔG_o), enthalpy (ΔH_o), and entropy (ΔS_o) from the thermodynamic study indicated that Co (II) adsorption by cuttlebone was feasible and endothermic at 20-40 °C [24].

Beside heavy metals ion adsorption, fluoride ions removal by cuttlebone has been investigated and the optimal conditions determined (contact time, pH effect, adsorbent dose, and initial fluoride concentration). The efficiency of cuttlebone in fluoride removal was 80 %, from an initial concentration of fluoride at 5 mg/L in a synthetic sodium fluoride solution with a pH of 7.2, for one hour, with an adsorbent dose of 15 g/L. The specific surface area of the cuttlebone adsorbent measured 0.070±0.002 m^2/g, and the experimental pH at the zero point of charge (pH_{zpc}) was found to be and 9.8. Following this experiment, cuttlebone can be used to eliminate excess fluoride in natural water, according to World Health Organization (WHO) recommendations [25].

Various effective adsorbents, including cross-linked xanthated chitosan [59], polymerized banana stem [42], egg shell [56], filamentous fungus (*Rhizopus arrhizus*) [60], and Brazilian sawdust samples of *Caryocar* spp., *Manilkara* spp., and *Tabebuia* spp. [40], have been tested for possible application in the treatment of lead-acid battery manufacturing wastewater.

CHAPTER III
EXPERIMENTALS

3.1 Chemicals

Double-distilled water and various chemicals were used in this study; the latter are presented in Table 3.1.

Table 3.1 List of chemicals used in present study

Chemical	Company
Lead (II) nitrate; AR	Ajax Finechem
Chromium (III) nitrate; AR	Ajax Finechem
Nitric acid; AR	QRëC
Hydrochloric acid; AR	QRëC
Sodium hydroxide; AR	CARLO ERBA
Calcium hydroxide; AR	MERCK
Calcium carbonate; AR	MERCK
Iron (II) chloride; AR	ACROS

3.2 Instruments

The instruments used in this study are presented in Table 3.2.

Table 3.2 List of instruments used in present study

Instrument	Manufacture
Oven	BINDER, ED/FD; Germany
Furnace	Nebertherm, LT 15/12; Germany
Fourier Transform infrared spectrometer	PerkinElmer, Spectrum One; USA
Surface area analyzer	Quantachrome, Autosorb-1; USA
Scanning electron microscope with energy-dispersive spectrometer attachment	JEOL, JSM-6610LV, and Link ISIS series 300; USA
X-ray diffractometer	Bruker AXS, Diffratometer D8; Germany
Refrigerated orbital incubator	SANYO GALLENKAMP PLC, IOC400.XX2.C; UK
pH meter	DENVER, pH/mV/Temp. Meter Model UB-10; USA
Flame atomic absorption spectrophotometer	Agilent, 240AA; USA
pH-conductivity-dissolved oxygen meter	HACH, sens ion 156; USA
Cool incubator	WTB BINDER, KBW; Germany

3.3 Experimental method

3.3.1 Preparation of adsorbent

The cuttlebones were naturally collected from the Lamchareon and Maerumpueng sea coasts in the Rayong province of Thailand. The specimens were washed and oven-dried at 80 ºC, then crushed and sieved to a particle size of less than 106 µm (Endecotts; England). The cuttlebone powder (CB-P) was rinsed with distilled water and dried at 60-80 °C for later use.

The modified adsorbent was prepared by carbonization of 5.0 g cuttlebone powder (< 106 µm) at 400 °C for two hours in a furnace (Nebertherm, LT 15/12; Germany). The result (CB-M400) was weighed and investigated for remaining mass after heat degradation loss.

All adsorbents used in this study were oven-dried at 60-80 °C and cooled in a desiccator before experiments.

3.3.2 Physicochemical characteristic of adsorbent

1) Functional group

The CB-P and CB-M400 were demineralized using diluted 1 M HCl solution at ambient temperature for three hours to a solution and adsorbent ratio of 40 mL/g. Thereafter, the precipitates were washed with distilled water, dried, and weighed. The calcium carbonate content and extracted content were evaluated from the weight of the adsorbent and precipitate, as represented by equations (3.1) and (3.2). The functional groups of the adsorbents and extracted contents were measured under a Fourier Transform infrared spectrometer (PerkinElmer, Spectrum One; USA).

$$\% \text{ Mineral content} = \frac{A-B}{A} \times 100 \quad (3.1)$$

$$\% \text{ Extracted content} = \frac{B}{A} \times 100 \quad (3.2)$$

Where A is the initial weight of adsorbent (g)

B is the weight after demineralization (g)

2) Surface structure

The Brunauer-Emmett-Teller (BET) specific surface area and total pore volume of CB-P and CB-M400 were determined by a surface area analyzer (Quantachrome, Autosorb-1; USA), with nitrogen gas adsorbate at 120.0 °C.

The surface structure and element of the adsorbents before and after adsorption of Pb (II), were measured by a scanning electron microscope with energy-dispersive spectrometer attachment (JEOL, JSM-6610LV, and Link ISIS series 300; USA). The chemical crystal structures of the adsorbents were qualitatively and quantitatively analyzed by an x-ray diffractometer (Bruker AXS, Diffratometer D8; Germany) at 40 kV and 40 mA, with a diffraction angle (2θ) of 10°-80° and a speed of 0.5 sec/step.

3.3.3 Adsorption experiment

All experiments were conducted with three replications of the batch process. Wastewater and a certain dose of the adsorbents (CB-P and CB-M400) were mixed for a fixed time in acid-washed glassware and separated from the wastewater by filtration. The Pb (II) concentration of the wastewater without adsorbents, and the separated wastewater after adsorption, were analyzed as the initial and final Pb (II) concentrations, respectively. The adsorption capacity and

efficiency, which were calculated using equations (3.3) and (3.4), were used to compare the study's quantity of Pb (II) adsorption.

$$q_e = \frac{(C_i - C_e)}{S} \quad (3.3)$$

$$E = \frac{C_i - C_f}{C_i} \times 100 \quad (3.4)$$

Where q_e is adsorption capacity (mg/g)

E is adsorption efficiency (%)

C_i is initial Pb (II) concentration (mg/L)

C_f is final Pb (II) concentration (mg/L)

S is concentration of adsorbents in mixing solution (g/L)

3.3.4 Effect of controlling factors on Pb (II) adsorption

The synthetic wastewater, diluted from stock Pb (II) solution at 10000 mg/L that was prepared from $Pb(NO_3)_2$ in HNO_3 0.5 N, were mixed with adsorbents by shaking at 100 rpm for 240 minutes at 30 °C in a refrigerated orbital incubator (Sanyo Gallenkamp PLC, IOC400.XX2.C; UK). After this, the adsorbents were separated from the wastewater using filter papers (Whatman No. 5) and the conditions of the Pb (II) adsorption were studied.

1) Effect of initial pH

The solution's pH was measured by a pH meter (Denver, pH/mV/Temp. Meter Model UB-10) and adjusted using NaOH and HNO_3. The adsorbents' particles after contact with a solution of pH 1.0-5.0 without Pb (II) ions, using an initial dose of 10 g/L, were dried and weighed.

For the adsorption experiment, the initial pH of the synthetic wastewater was adjusted to 1.0-5.0, while the adsorbent dose and Pb (II) initial concentration in the wastewater were fixed at 0.5 g/L and 500 mg/L, respectively. The pH of the synthetic wastewater after adsorption was detected.

2) Effect of adsorbent dose and initial Pb (II) concentration

The adsorbent dose was valued within a range of 0.1-0.7 g/L, and each dose was augmented with Pb (II) synthetic wastewater at an initial concentration of 10-1000 mg/L; this adjusted the initial pH to an optimum level. After 240 minutes, the adsorption reaction was assumed to be in the equilibrium state. The adsorption capacity and final Pb concentration were used in the adsorption equilibrium model, with a linear form of Langmuir isotherm and Freundlich isotherm, following equations (3.5) and (3.6), respectively.

$$\frac{C_e}{q_e} = \frac{1}{K_L q_m} + \frac{C_e}{q_m} \qquad (3.5)$$

$$\log q_e = \log K_F + \frac{1}{n}\log C_e \qquad (3.6)$$

Where C_e is the Pb (II) concentration at the equilibrium (mg/L)

q_e is the adsorption capacity at the equilibrium (mg/g)

K_L is the Langmuir isotherm constant (L/mg)

K_F is the Freundlich isotherm constant ((mg/g)·(L/g)^n)

q_m is the maximum adsorption capacity (mg/g)

n is the adsorption intensity

3.3.5 Adsorption kinetic

0.2 g of adsorbents were added to 1 L of 100 and 500 mg/L Pb (II) synthetic wastewater with a pH of 4 and mixed at 200 rpm using a magnetic stirrer bar at 30 °C in a cool incubator (WTB BINDER, KBW). 1 mL of the solution was sampled at 15-360 minutes by filtrating it using a syringe filter with a pore size of 0.45 µm (Advantec, 25CS045AN), and analyzed for Pb (II) concentration. The pseudo-first-order, pseudo-second-order, and intra-particle diffusion kinetic model proscribed by equations (3.7), (3.8), and (3.9), respectively, were used to analyze the experimental data.

$$\ln(q_e - q_t) = \ln q_t - K_1 t \quad (3.7)$$

$$\frac{t}{q_t} = \frac{t}{q_e} + \frac{1}{k_2 q_e^2} \quad (3.8)$$

$$q_t = K_{int}\sqrt{t} \quad (3.9)$$

Where q_e is the adsorption capacity at the equilibrium (mg/g)

qt is the adsorption capacity (mg/g) at time t (minute)

K_1 is the pseudo-first-order rate constant (s-1)

K_2 is the second-order rate constant (g/(mg·minute))

K_{int} is the intra-particle diffusion rate constant (mg/(g·minute$^{1/2}$))

3.3.6 Adsorption interference

The Pb (II) adsorption interference was investigated as a Pb (II) adsorption kinetic study. The adsorbents were added to combine heavy metals with synthetic wastewater, which was mixed using Pb (II) synthetic wastewater and an interference ion (Fe (II) or Cr (III)) to a mole ratio of 1:1. The solution was collected at a time between 5-360 minutes in order to analyze Pb (II).

3.3.7 Battery wastewater treatment procedures

The dissolved wastewater, separated by glass microfiber filters (Whatman GF/F), was used in fixed chemicals and an adsorbents experiment, using the three treatments shown in Table 3.3. All treatments were performed at a shake speed of 100 rpm at 30 °C for 240 minutes. The treatments for the wastewater quality parameters shown in Table 3.4 were measured and compared with the industrial effluent standards limit.

3.3.8 Data analysis

Mean and standard deviation of the quantity scale experimental results were calculated from three replicated datasets. The comparison between dependent factors was tested using one-way analysis of variance (ANOVA) and Duncan multiple range test (DMRT), with a 95 % confidence interval. The correlation coefficient (R^2) was analyzed using a descriptive linear regression model.

Table 3.3 Battery wastewater treatments

Treatment	Adjusted pH	Adsorbent	Dose (g/L)
I	-	CB-P, CB-M400	0.2-10.0
II	4.0 by NaOH	CB-P, CB-M400	0.2-1.0
III	$Ca(OH)_2$	CB-P, CB-M400, $Ca(OH)_2$, $CaCO_3$	0.2-1.0

Table 3.4 Wastewater quality parameters measurement

Wastewater quality parameter	Measurement
pH	pH meter
Total dissolved solid (TDS)	pH-conductivity-dissolved oxygen meter (HACH, sens ion 156; USA)
Heavy metals - Lead (Pb) - Iron (Fe) - Chromium (Cr) - Nickel (Ni) - Zinc (Zn) - Manganese (Mn)	Flame atomic absorption spectrophotometer (Agilent, 240AA; USA)

CHAPTER IV
RESULTS AND DISCUSSION

4.1 Physicochemical characteristics of adsorbent

4.1.1 Functional group

CB-P and CB-M400 were decalcified using HCl. The proportion of minerals and extracted content in the adsorbents is shown in Table 4.1. Functional groups of the adsorbents and extracted content were analyzed; their FTIR spectra are presented in Figure 4.1. More than 90 % of the adsorbents' composition was mineral content. Besides the band characteristic, major peaks of 1475, 856, and 713 cm^{-1} of CO_3^{2-} vibration in CB-P, and 1424, 875, and 713 cm^{-1} in CB-M400 were found [61]. There were minor peaks of 2522, 1789, and 1083 cm^{-1} for $CaCO_3$ (aragonite) in CB-P (see Figure 4.1 (a)), 2513 and 1798 cm^{-1} for $CaCO_3$ (calcite) in CB-M400 (Figure 4.1 (b)), and 3424 and 3437 cm^{-1} for water molecules of crystallization [61].

While $CaCO_3$ is the main component of cuttlebone, it also features organic content of β-chitin and proteins to a lesser extent [20, 21]. The absorption peaks of the extracted content of CB-P (Figure 4.1 (c)) show a broad peak of O-H stretching to 3400 cm^{-1}, C-O stretching to 1033 cm^{-1} and 1068 cm^{-1}, and C-O-C stretching to 1155 cm^{-1}. The functional groups of chitin and protein were presented in C=O bonded amide stretching at 1656 cm^{-1} and 1650 cm^{-1}, N-H bending of amine at 3096 $cm^{-1}$and 1546 cm^{-1}, C-N stretching at 1312 cm^{-1}, and amide III at 1233 cm^{-1} and 1205 cm^{-1} [20, 21]. Absorption bands of extracted content from CB-M400 (Figure 4.1 (d)) were shown, with broad peaks appearing at 3391 cm^{-1} for O-H stretching, 1594 cm^{-1} for N-H bending, and 1217 cm^{-1} for C-N stretching. The organic carbon bond peaks, such as 1656 cm^{-1} and 1649 cm^{-1} of C=O, 1413 cm^{-1} of C-H, 1377 cm^{-1} of C-CH_3, and 1155-1033 of C-O, as seen in CB-P, had disappeared.

Table 4.1 Mineral content and extracted content of adsorbents

Adsorbent	Mineral content (% ± SD)	Extracted content (% ± SD)
CB-P	97.23 ± 0.10	2.77 ± 0.10
CB-M400	99.59 ± 0.07	0.41 ± 0.07

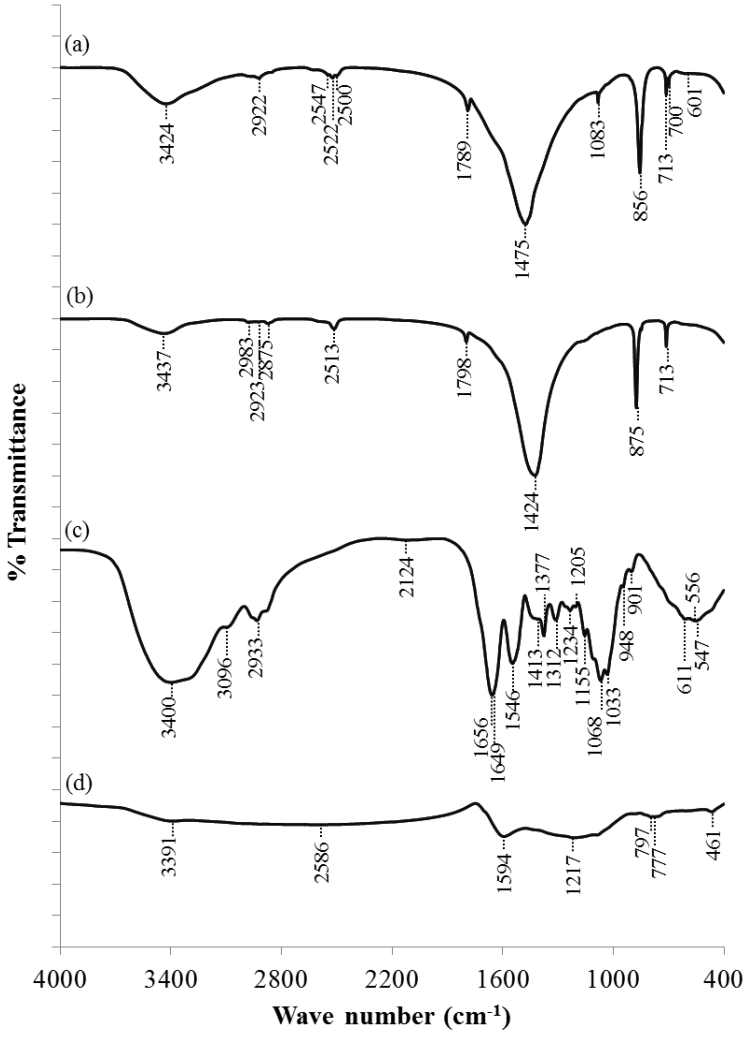

Figure 4.1 FITR spectra of CB-P (a), CB-M400 (b), extracted contents from CB-P (c), and extracted contents from CB-M400 (d)

4.1.2 Surface structure

As analyzed by SEM-EDS, the surface structures of adsorbents before and after Pb (II) adsorption are presented in Figures 4.2 and 4.3, respectively. Before Pb (II) adsorption, the CB-P surface was corrugated and rough, while that of CB-M400 was smooth. Table 4.2 shows the surface analysis of CB-P and CB-M400, disclosing that the specific surface, pore volume, and pore size of the former were higher than those of the latter. After Pb (II) adsorption, both adsorbents' surfaces were covered with chemical crystals. As indicated by Table 4.3, Ca, C, and O were major elements in both adsorbents, and Pb was observed on both their surfaces after adsorption (70.50 % in CB-P and 65.32 % in CB-M400). The crystalline structures of both were confirmed using XRD technique. Figure 4.4 displays the XRD patterns of the adsorbents before and after Pb (II) adsorption. The quantity of each crystalline is analyzed and presented in Table 4.4. Aragonite was major components in CB-P, whereas only calcite was detected in CB-M400. Take-up Pb (II) adsorbents were identified as follows: $PbCO_3$ and $Pb_3(CO_3)_2(OH)_2$ with aragonite in CB-P and calcite in CB-M400.

Observed corrugate surface on CB-P was thin film layer of organic are coat inorganic matter of cuttlebone [17]. Some rough surface was effect of calcium carbonate dissolution by distill water and mechanical force from adsorbent preparing method. Heat in carbonization process affects to CB-M400 physical and chemical properties. Reducing surface area and pore volume of CB-M400 was resulted from organic contents thermal degradation in CB-P

The crystalline aragonite in CB-P was thermal transformed to calcite in CB-M400. For $CaCO_3$ composition, the transformation of $CaCO_3$ was founded in thermal degradation of cuttlebone [20, 21] and conch shell (*Busycon carica*) [62]. With approximate temperature, organic contents is burned out at 225-330 °C, while aragonite structure of $CaCO_3$ is thermal transformed to calcite at 407-550 °C, then degraded to CaO and CO_2 at 607-900 °C [20, 21, 62]. In CB-M400 preparation, 5.36 ± 0.01 % of weight was lost due to burning out of volatile carbon in CB-P. According to study of Birchall and Thomas [17], Klungsuwan [21], cuttlebone was contained 3-7 % β-chitin. Therefore,

carbonization of organic matter in CB-P was assumed by chitin thermal decomposition. From thermogravimetric analysis of chitin, the major amount of volatiles was released at 150-315 °C [63]. While, 45-73 % of chitin weigh was lost by volatile degradation at 320-350 °C, and amount of carbonized residue was not exceed 8-10 % at 900 °C [19, 63]. Therefore, effect of thermal gravimetric on chitin indicated that the remaining of extracted content in CB-M400 was fixed carbon.

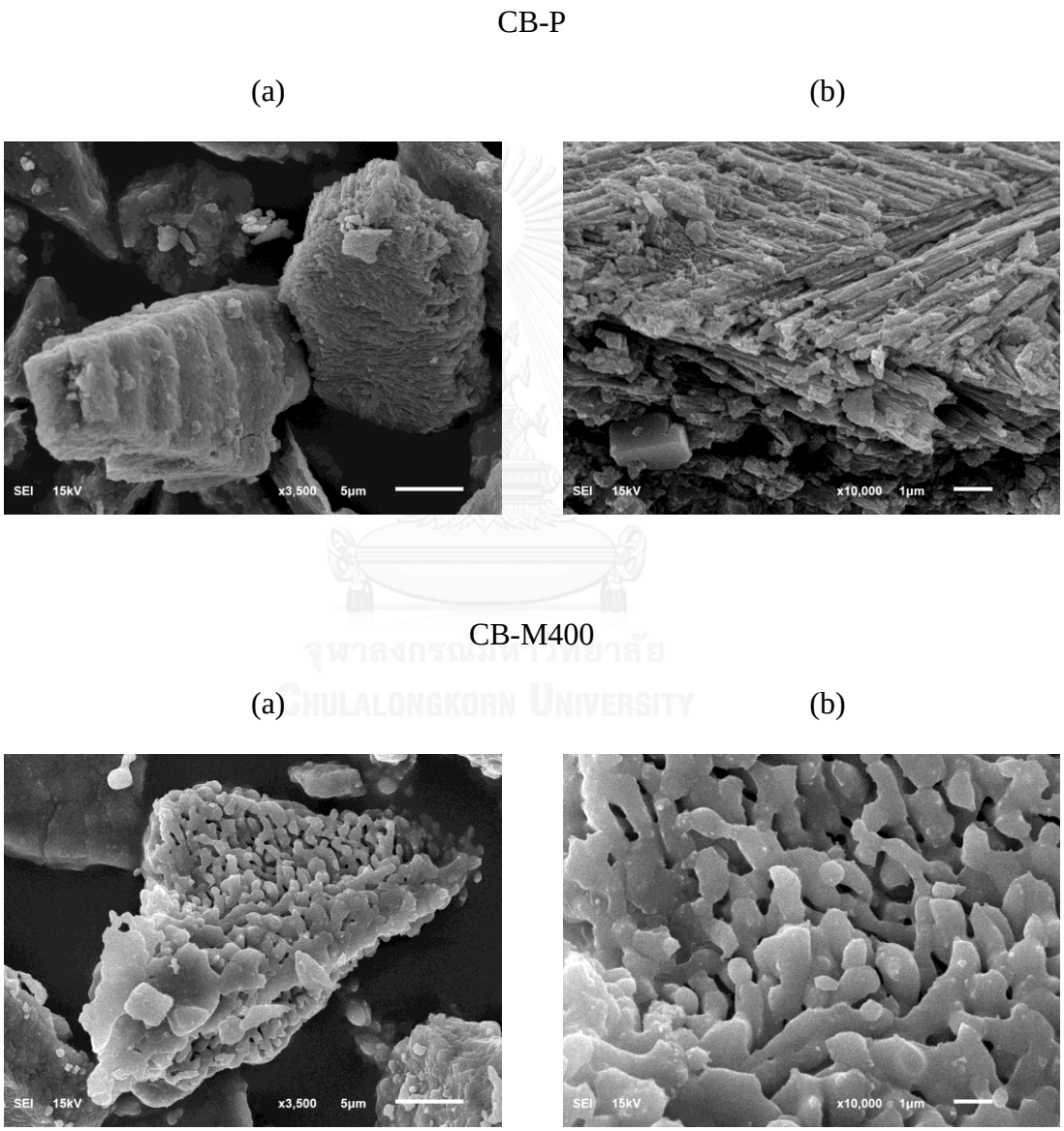

Figure 4.2 Surface structures of CB-P and CB-M400 before Pb (II) adsorption, at a magnification of 3,500x (a) and 10,000x (b) by SEM-EDS

CB-P

(a) (b)

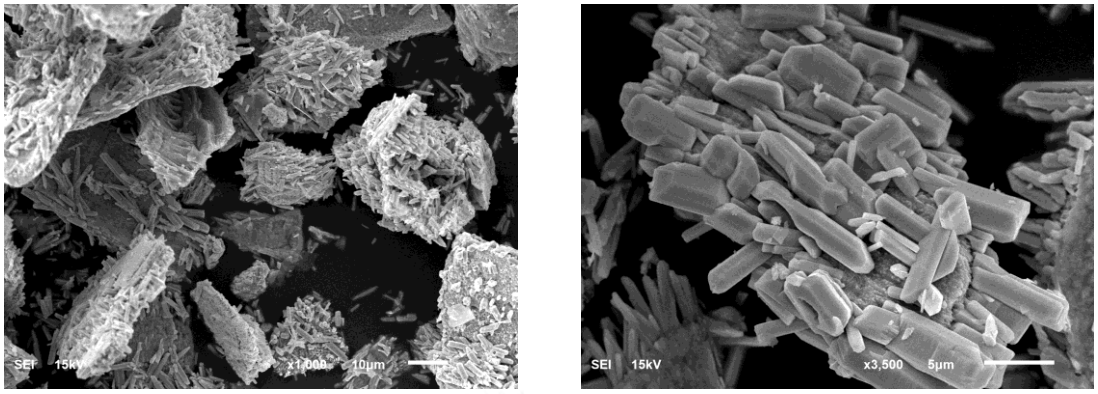

CB-M400

(a) (b)

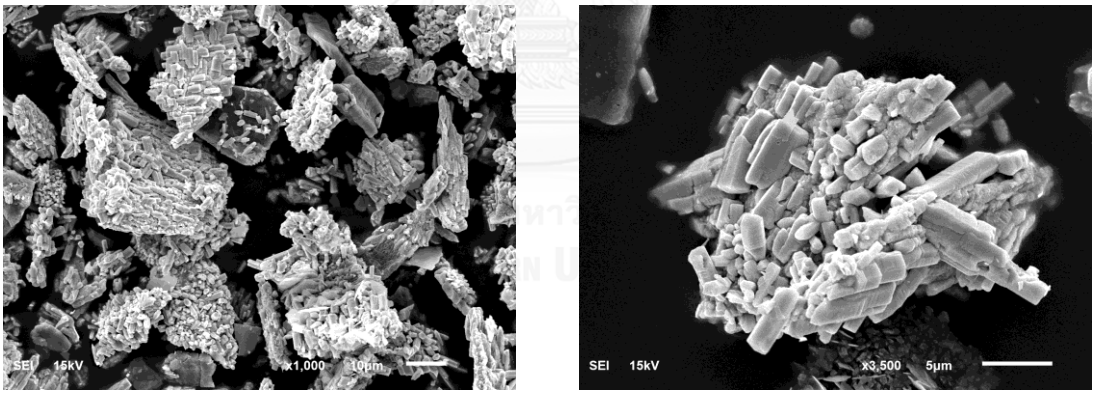

Figure 4.3 Surface structures of CB-P and CB-M400 after Pb (II) adsorption* at a magnification of 1,000x (a) and 3,500x (b) by SEM-EDS

* Using synthetic wastewater with Pb (II) of 500 mg/L, at a pH of 4.0, with an adsorbent dose of 0.2 g/L, for 360 minutes at 30 °C

Table 4.2 Surface analysis using surface area analyzer

Adsorbent	Specific surface area* (m^2/g)	Pore volume (cc/g)	Pore size (Å)
CB-P	8.41	0.0201	95.51
CB-M400	2.69	0.0043	64.49

*Multipoint BET

Table 4.3 Elements on adsorbents' surfaces before and after adsorption of Pb (II) by SEM-EDS

Element	CB-P		CB-M400	
	Before (% wt/wt)	After (% wt/wt)	Before (% wt/wt)	After (% wt/wt)
C	25.02	17.80	16.33	16.10
O	51.66	9.89	49.89	17.32
Na	0.77	-	1.03	-
Mg	-	-	0.62	-
Cl	0.73	-	0.24	-
Ca	21.83	1.80	31.90	1.26
Pb	-	70.50	-	65.32

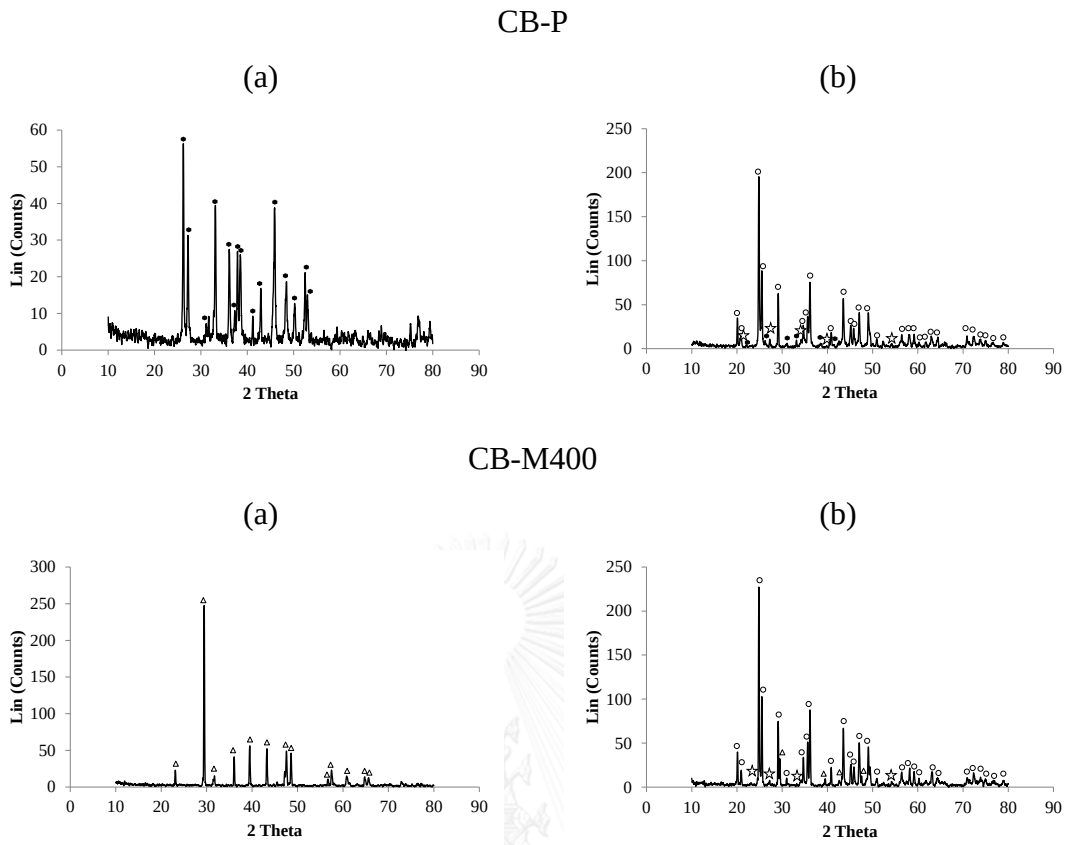

Figure 4.4 XRD patterns of $CaCO_3$ aragonite (⬢), $CaCO_3$ calcite (△), $PbCO_3$ (○), and $Pb_3(CO_3)_2(OH)_2$ (☆) in CB-P and CB-M400, before (a) and after Pb (II) adsorption (b) *

Table 4.4 Quantitative analysis of crystalline in CB-P and CB-M400

Crystalline	Before Pb(II) adsorption		After Pb(II) adsorption*	
	CB-P	CB-M400	CB-P	CB-M400
$CaCO_3$ (aragonite)	98.93 %	-	23.92 %	-
$CaCO_3$ (calcite)	0.74 %	100.00 %	-	31.20 %
NaCl	2.34 %	-	-	-
$PbCO_3$	-	-	74.84 %	67.52 %
$Pb_3(CO_3)_2(OH)_2$	-	-	1.24 %	1.29 %

* Using synthetic wastewater with Pb (II) of 500 mg/L, at a pH of 4.0, with an adsorbent dose of 0.2 g/L, for 360 minutes at 30 °C

As observed from the elemental data, both adsorbents are $CaCO_3$-rich material. Therefore, the mechanism of Pb removal may be modeled as consisting of $CaCO_3$ bio-material, such as crab shell and egg shell adsorbents, which is explained by $PbCO_3$ micro-precipitation on the surface and chitin composite chelating of the precipitate $PbCO_3$. The dissolution of $CaCO_3$ in the crab shell formed CO_3^{2-} and HCO_3^- in the solution; they reacted with Pb in the solution to become $PbCO_3$ and $Pb_3(CO_3)_2(OH)_2$, which were precipitated and adsorbed to chitin on the surface. [49]

After Pb (II) adsorption, the discovery of crystalline $PbCO_3$ and $Pb_3(CO_3)_2(OH)_2$ was confirmed by Pb (II) precipitation by CO_3^{2-} on the adsorbent surface. Some $CaCO_3$ remained, namely aragonite in CB-P and calcite in CB-M400, indicating particular adsorbents in the adsorption process and supporting Pb's precipitate adsorption on the surface. A small detected amount of chitin and organic protein contents in CB-P and fixed carbon content in CB-M400 in the functional group characterization emphasized the function for chelate or the adsorption of Pb precipitate compounds.

From the surface structure analysis results, $CaCO_3$ was present in both adsorbents before Pb take-up; Pb crystalline compounds were measured on the CB-P and CB-M400's surfaces after Pb adsorption. The analyzed data suggests $PbCO_3$ and $Pb_3(CO_3)_2(OH)_2$ micro-precipitation and precipitate adsorption on the adsorbents' surfaces, as follows:

$$\text{Adsorbents} + H_2O \rightarrow \text{Adsorbents} + Ca^{2+} + CO_3^{2-} \quad (4.1)$$

$$CO_3^{2-} + H_2O \leftrightarrow HCO_3^- + OH^- \quad (4.2)$$

$$Pb^{2+} + CO_3^{2-} \rightarrow PbCO_{3(s)} \quad (4.3)$$

$$3Pb^{2+} + 2CO_3^{2-} + 2OH^- \rightarrow Pb_3(CO_3)_2(OH)_{2(s)} \quad (4.4)$$

$$\text{Adsorbent} + \text{Pb Complexes} \rightarrow \text{Adsorbent} - \text{Pb} \quad (4.5)$$

4.2 Effect of controlling factors on lead removal

4.2.1 Effect of initial pH

The effect of the initial pH on the adsorbent is shown in Figure 4.5 as a percentage of the particulate adsorbent and dissolved matter in different pH values of aqueous solution. Most particulate adsorbents remained in the solution at a pH of 2.0-5.0, but at pH 1.0, 25.94 ± 0.92 % and 1.12 ± 0.35 % of CB-P and CB-M400 were particles. Figure 4.6 presents the effect of pH on Pb (II) adsorption's capacity and efficiency, whose values shared the same trend with a low value pH of 1.0-2.0, increasing with pH 3.0-4.0, and changing little at pH 5.0. In overall adsorption capacity and efficiency, CB-P was similar to CB-M400; that is, there was no statistical difference with a 95 % confidence interval. As a comparison between each initial pH, the difference the adsorbents' capacity and efficiency at pH 1.0 and 2.0 were not significant; there was also no appreciable difference at pH 4.0 and 5.0. At pH 1.0 and 2.0, the capacity and efficiency of CB-M400 were significantly higher than those of CB-P. Changing the pH (ΔpH) of synthetic wastewater after Pb (II) adsorption, as shown in Figure 4.7, increased them to a higher value than at the initial pH, with a peak at an initial pH of 3.0 in CB-P and 4.0 in CB-M400.

The solution's pH strongly affected the Pb (II) adsorption of CB-P and CB-M400. From the abovementioned physicochemical characteristic of adsorbent analysis, cuttlebone, consisting of $CaCO_3$ and CO_3^{2-}, played a mainly functional role in Pb (II) adsorption. The $CaCO_3$ and CO_3^{2-} chemical equilibrium was related to the solution's pH, as follows:

$$CaCO_3 \rightarrow Ca^{2+} + CO_3^{2-} \quad (4.6)$$

$$CO_3^{2-} \leftrightarrow HCO_3^- \leftrightarrow H_2CO_3 \leftrightarrow CO_2 + H_2O \quad (4.7)$$

As per Le Chatelier's principle, a chemical system will respond to changes in its processes, which tends to reduce the effect of the changes [3, 5]. For the $CaCO_3$ and CO_3^{2-} equilibrium, a high concentration of H^+ in a low-pH solution

induced a reaction shift in CO_3^{2-} to HCO_3^-, as well as in H_2CO_3 to CO_2, which generated optical bubbles gas. This reaction shift was the cause of more dissolution of $CaCO_3$ to CO_3^{2-}, which passed to HCO_3^- and H_2CO_3; this showed as a high percentage of dissolved adsorbents' matter and resulted in reduced efficiency of Pb (II) adsorption. Therefore, a higher percentage of $CaCO_3$ and fixed carbon content in CB-M400 would be rather more effective in removing Pb (II) in a low-pH solution than the organic contents of CB-P.

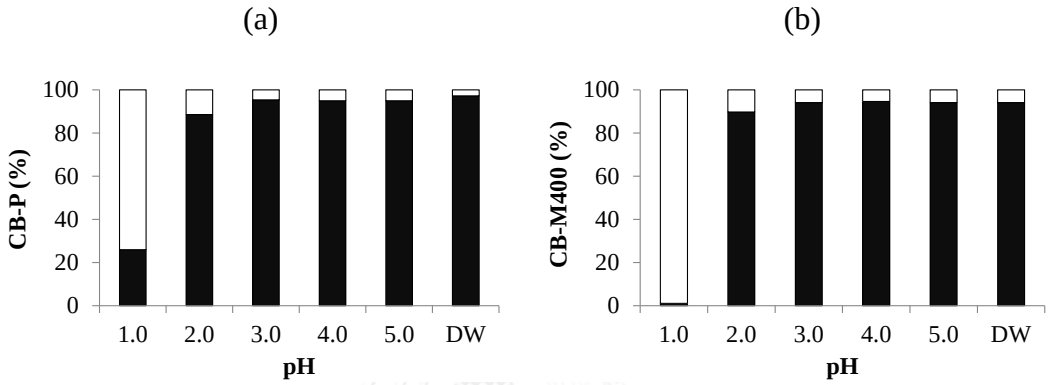

Figure 4.5 Percentage of particulate adsorbent (■) and dissolved matter (□) of CB-P (a) and CB-M400 (b) in aqueous solution at a pH of 1.0-5.0 and distilled water (DW)

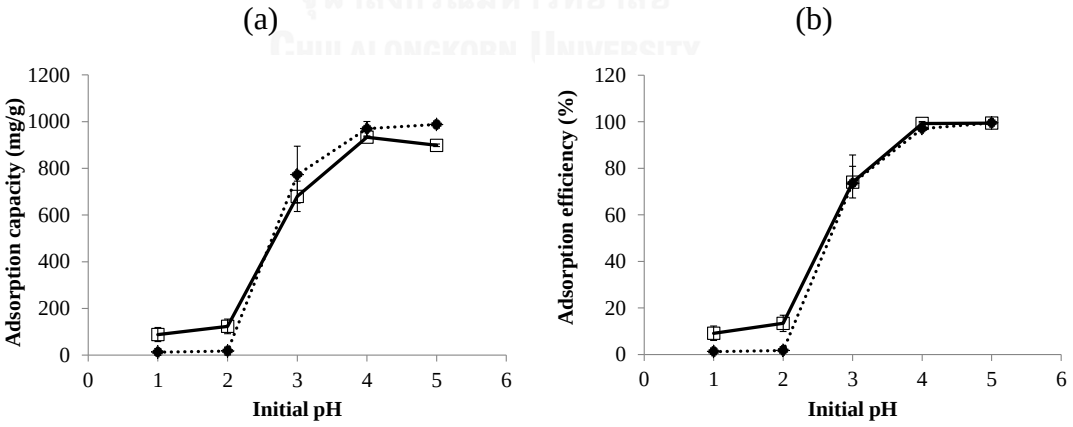

Figure 4.6 Effect of initial pH on Pb (II) adsorption capacity (a) and efficiency (b) in CB-P (◆) and CB-M400 (□)

* Using synthetic wastewater with Pb (II) at 500 mg/L, at an adsorbent dosage of 0.5 g/L, for 360 minutes at 30 °C

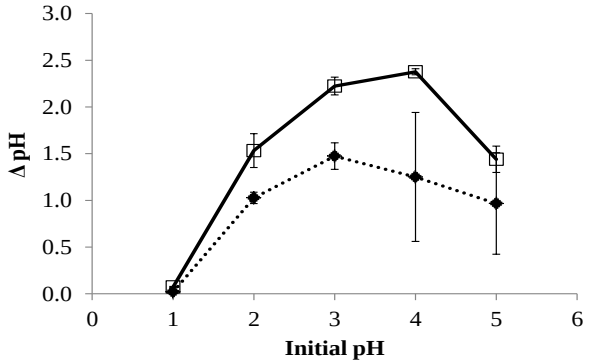

Figure 4.7 Altered pH (ΔpH) of synthetic wastewater after Pb (II) adsorption by CB-P (◆) and CB-M400 (□)

The phenomenon of protonation/deprotonation on adsorbents' surfaces also explains the relationship between the adsorbent and the solution's pH, in which the functional group dissociates and causes a competition between the targeted ion and H^+ or H_3O^+ ion. As presented in the algal biomass [31-33] and plant biomass residues [36-40, 42], the organic active site for cation adsorption will be protonated by a high concentration of H^+ or H_3O^+ ions and becomes less available for binding heavy metals in a low-pH solution. A changed pH value after the adsorption process (ΔpH) expresses the removal of H^+ from the solution. While the initial pH is 1.0, a high concentration of H^+ produces H_2CO_3, then shifts to CO_2; some of this is adsorbed on non-$CaCO_3$ contents, with the result that the pH is slightly increased and less ΔpH is presented. For an initial pH of 2.0 and 3.0, the system balance of H^+ with CO_3^{2-} reacts to HCO_3^- and H_2CO_3, increasing the ΔpH. Higher ΔpH in CB-M400 is the reason for greater $CaCO_3$ content in CB-M400, which was more dissolved than CB-P. With an initial pH of 4.0 and 5.0, a resistant pH-changing buffer property of the CO_3^{2-}, HCO_3^-, and H_2CO_3 equilibrium occurs as the ΔpH decreases and the final pH changes slightly.

The pH at zero point of charge (pH_{zpc}) gives a more adequate explanation for the effect of pH, which has a neutral charge on the adsorbent's surface. When the solution pH is higher than pH_{zpc}, the surface will be negatively charged. In contrast, when the solution pH is lower than pH_{zpc}, the surface will be positively charged [24, 25]. Based on Sandesh *et al.*, an experimental pH_{zpc} of the

cuttlebone, valued at 9.7,was discovered [24]. This pH_{zpc} data could be considered as a highly acidic condition on the adsorbent's surface, posing a more positive charge that loses some active sites for Pb (II) adsorption.

Due to the battery wastewater's pH (valued at 0.7) and heavy metals contamination in the acidic condition of wastewater, experiments must be performed in acid conditions. To avoid heavy metals hydroxide precipitation, which may occur with a high pH solution, the next round of experiments will be conducted at an optimum initial pH value of 4.0, which yields high capacity and efficiency.

4.2.2 Effect of adsorbent dose and Pb (II) initial concentration

Figure 4.8 shows the effect of the adsorbents' dose and an initial concentration of Pb (II) in synthetic wastewater with an adsorption capacity and efficiency of CB-P and CB-M400 of 0.2-0.7 g/L in a Pb (II) concentration of 10-1000 mg/L. The capacity and efficiency of both adsorbents, overall, shared the same direction, although CB-M400 had a slightly higher value in a non-statistical sense. In low concentrations of Pb (II) solution (10 and 100 mg/L), capacity was significantly reduced when adding more adsorbents and when 100 % of Pb (II) ions were removed. Conversely, in higher concentrations (250 and 500 mg/L), capacity increased to peak at 0.2 g/L. With an extremely high concentration (1000 mg/L), the capacity was not different in each adsorbent dosage in CB-P, while there was a small decrease in the inversely adsorbent dose in CB-M400. The capacity of CB–M400 was clearly significantly higher than that of CB-P.

The effects of the dose and the heavy metal ions' initial concentration were related to the surface area, a number of active sites, functional dissociation, and the amount of heavy metal ions in the solution. The adsorbent surface area was strongly correlated to the active binding site. Under closer examination, there was a reduction in the efficiency of removal in smaller surface areas of larger-sized adsorbents [24, 51, 54, 57, 58, 60].

In terms of an overview of each concentration, the capacity increased when using a higher concentration, and the removal efficiency was reversed [9, 36, 37, 39, 42, 46, 47, 50, 53-56, 58]. At a low concentration, the addition of a greater dose resulted in a smaller capacity and greater efficiency because most heavy metal ions were adsorbed in the solution and there still remained available active sites in the adsorbents without heavy metal binding [9, 23-25, 42, 45, 51, 56-58, 60]. With a high concentration, there was a greater capacity but not all heavy metal ions were removed. The capacity and adsorbents dose increased in parallel in the earliest stage, but the capacity reduced when using a higher dose, causing a low functional dissociation on the reduced surface area from the partial aggregation of a high-density adsorbent [31, 37-39]. At an extremely high concentration, a higher capacity in CB-M400 was most likely the effect of its $CaCO_3$ and fixed

carbon contents. However, the denaturation of the organic contents resulted in inactivity regarding the removal of Pb in CB-P. According to the peak capacity of the adsorbents in Pb (II), 250 and 500 mg/L, the optimum dose was 0.2 g/L.

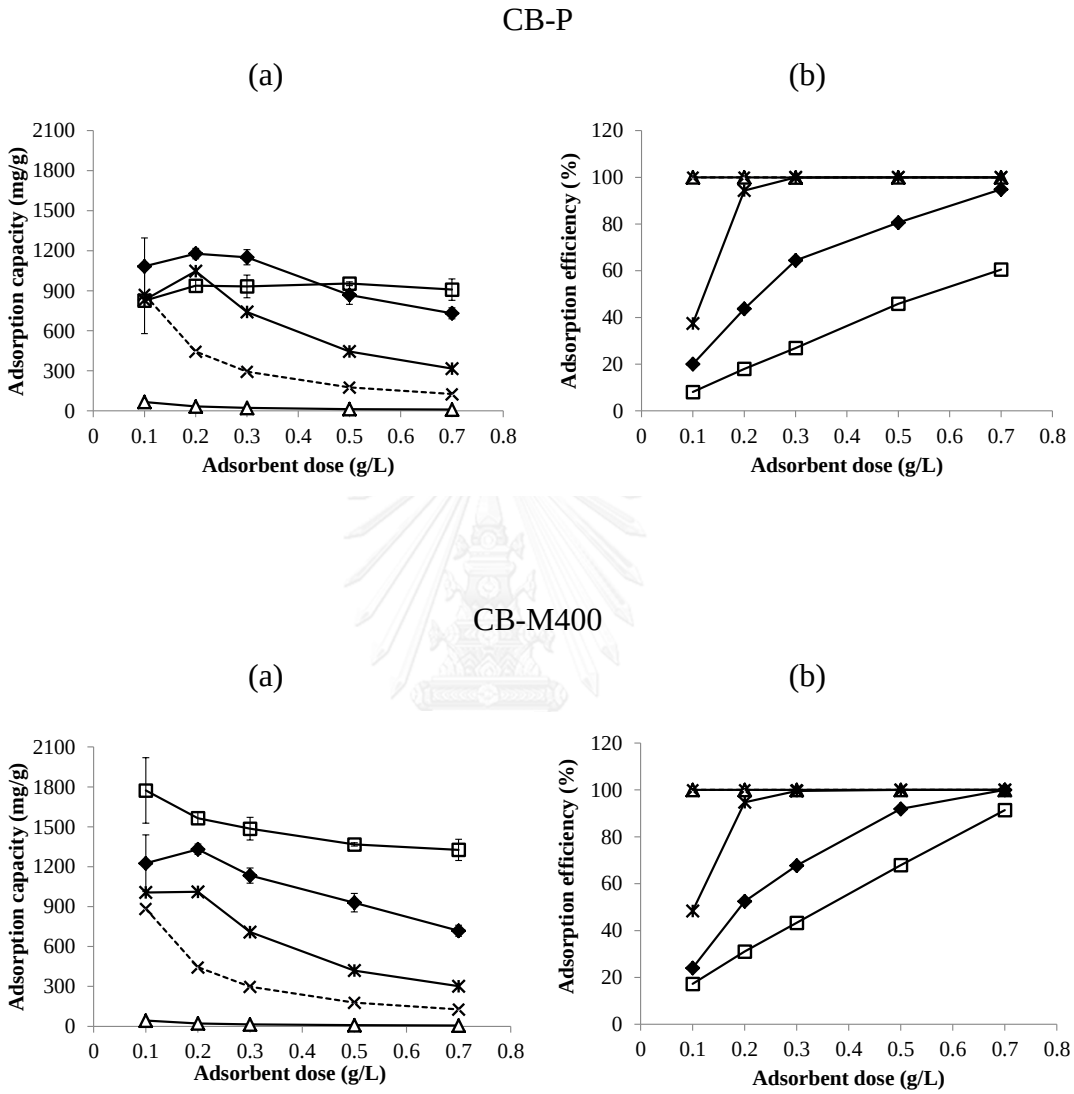

Figure 4.8 Effect of adsorbents dosage and Pb (II) initial concentration in adsorption capacity (a) and adsorption efficiency (b) of CB-P and CB-M400

* Using synthetic wastewater with Pb (II) of 10 mg/L (△), 100 mg/L (×), 250 mg/L (∗), 500 mg/L (◆), and 1000 mg/L (□), at a pH of 4.0, with an adsorbent dosage of 0.1-0.7 g/L, for 360 minutes at 30 °C

4.3 Adsorption isotherms

The Langmuir and Freundlich isotherms have been the most widely used models for describing the solid-liquid adsorption equilibrium [7]. The Langmuir isotherm assumes a monolayer adsorption with a thin layer on the adsorbent surface, or chemical adsorption that only occurs at a fixed number of specific adsorption sites; there is no lateral interaction between the adsorbed molecules and homogeneous adsorption, which has constant enthalpies and activation energy. Meanwhile, the Freundlich isotherm assumes non-ideal reversible adsorption or multilayer adsorption, with a heterogeneous surface [7, 8]. Table 4.4 shows the Langmuir and Freundlich isotherm parameters for the Pb (II) adsorption of CB-P and CB-M400. The correlation coefficient (R^2), which predicts the trend of a linear model isotherm, was more than 0.9 in the Langmuir isotherm analysis. This result affirms that the Langmuir isotherm is more suitable for our purposes than its Freundlich counterpart. Maximum Pb (II) adsorption capacity (q_m), as estimated from the Langmuir isotherm, was 869.57 mg/g in CB-P and 1573.56 mg/g in CB-M400.

The separation factor (R_L) could indicate the adsorption affinity, which had a strong irreversible reaction in CB-P ($R_L < 0$) and a favorable one in CB-M400 ($0 < R_L < 1$). The former was the cause of the binding of Pb by organic content. On the other side, a greater capacity of CB-M400, which relates to its higher $CaCO_3$ contents, posed a more reversible reaction by fixed carbon content adsorption. As shown in Table 4.5, the maximum Pb (II) capacities of CB-P and CB-M400 were clearly greater than those of various adsorbents found in the literature review.

As well as the Langmuir model and $CaCO_3$ micro-precipitation on the surface or adsorption of precipitates [23, 49-55, 57, 58], the equilibrium phenomenon of heavy metals' adsorption in $CaCO_3$ composite adsorbents may be combined with different descriptions. The Freundlich model [57] and Ca^{2+} ion exchange [23, 57] have been discussed in some heavy metals adsorption studies. Although the heavy metal adsorption equilibrium of cuttlebone adsorbents was a function of the temperature via the effect of the active binding site and exothermic reaction [24], it maintained efficiency at 15-45 °C and decreased at temperatures over 45 °C [23].

Table 4.5 Adsorption isotherm parameters

Adsorbent	Langmuir isotherm				Freundlich isotherm		
	q_m	K_L	R_L	R^2	n	K_F	R^2
CB-P	869.57	-0.1217	-0.0083	0.9329	15.67	657.7	0.5434
CB-M400	1573.56	0.0705	0.0140	0.9724	9.60	732.8	0.7512

Table 4.6 Comparison of maximum Pb (II) adsorption capacity

Adsorbent	pH	q_m (mg/g)	Reference
CB-M400	4.0	1573.56	This study
Crab shell (*Protunus trituberculatus*)	5.0	1300.00	[49]
CB-P	4.0	869.57	This study
Chicken eggshell powder	5.0	577.00	[54]
Crab shell (*P. sanguinolentus*) treated by HCl/NaOH	4.5	564.00	[58]
Cross-linked xanthated chitosan	4.0	322.60	[59]
Crab shell (*Chinonecetes opilio*)	5.0	267.29	[50]
Brown algae (*Cystoseira barbata*)	4.0	239.82	[33]
Sawdust (*Manilkara* spp.)	5.0	145.00	[40]
Minus duckweed (*Lemna perpusilla* Torr)	4.6	128.21	[37]
Sawdust (*Tabebuia* spp.)	5.0	95.00	[40]
Red algae (*Galaxaura oblongata*)	5.0	88.60	[31]
Green algae waste biomass (*Ulva lactuca* sp.)	5.0	66.43	[32]
Red algae (*Corallina mediterranea*)	5.0	64.30	[31]
Peanut shell	5.5	38.91	[39]
Red algae (*Pterocladia capillacea*)	5.0	34.10	[31]
Red algae (*Jania rubens*)	5.0	30.60	[31]

4.4 Adsorption kinetic

Figure 4.9 shows the adsorption capacity of CB-P and CB-M400 from 5-360 minutes with initial Pb (II) concentrations of 100 and 500 mg/L. With the latter, adsorption capacity from 5-360 minutes was not significant for either adsorbent. The adsorption capacity rapidly increased from 5-120 minutes for CB-P and from 5-60 minutes for CB-M400; thereafter, it changed slowly from 150-180 minutes for CB-P and from 90-240 minutes for CB-M400, before becoming stable and not statistically significant from 240-360 minutes for both adsorbents. With an initial Pb (II) concentration of 100 mg/L, the capacity of CB-P rose insignificantly from 5-20 minutes, then changed suddenly from 20-60 minutes and did not change after 60 minutes. This was different in the case of CB-M400, whereby the capacity was changed rapidly from 5-20 minutes then increased slightly before becoming stable; the capacity was lower than in the 500 mg/L experiment.

Capacity was in a stable state when the contact time was above 240 minutes for 500 mg/L and above 60 minutes for 100 mg/L, which indicates the adsorption equilibrium. As a result of the effect of the adsorbents dose and initial Pb (II) concentration, the adsorption capacity increased when there were more Pb (II) ions in the solution, due to the limited available surface area. In the kinetic study, the initial concentration affected the reaction rate and used the contact time to enter the equilibrium or finish the reaction.

Pseudo-first- and pseudo-second-order kinetic models were used to evaluate the reaction rate in the adsorption study [7, 10, 11]. Table 4.6 presents the Pb (II) adsorption kinetic model parameters for CB-P and CB-M400. The pseudo-second-order model was suitable for Pb (II) adsorption of both CB-P and CB-M400, with a correlation coefficient (R^2) that was higher than that of the pseudo-first-order model. The reaction rate constant of the pseudo-second-order model (K_2) inferred that its reaction rate was more valuable in initial Pb (II) concentration of 100 mg/L with CB-M400.

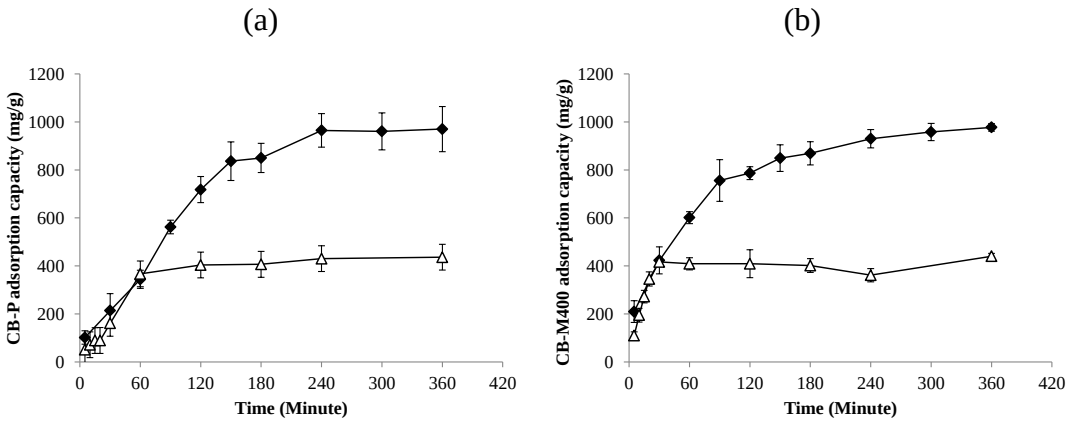

Figure 4.9 Adsorption capacities of CB-P (a) and CB-M400 (b) from 5-360 minutes

* Using synthetic wastewater with an initial Pb (II) concentration of 100 mg/L (△) and 500 mg/L (◆), at a pH of 4.0, with an adsorbent dosage of 0.2 g/L, at 30 °C

Table 4.7 Adsorption kinetic model parameters

Pb (II) (mg/L)	Adsorbent	Pseudo-first-order			Pseudo-second-order		
		K_1	q_e	R^2	K_2	q_e	R^2
100	CB-P	$1.74x10^{-2}$	401.82	0.9481	$3.14x10^{-5}$	528.82	0.9710
	CB-M400	$6.25x10^{-3}$	139.49	0.2391	$2.59x10^{-4}$	426.26	0.9867
500	CB-P	$1.74x10^{-2}$	1388.53	0.9016	$6.41x10^{-6}$	1340.12	0.9241
	CB-M400	$1.23x10^{-2}$	829.65	0.9912	$2.38x10^{-5}$	1075.62	0.9958

Figure 4.10 illustrates the internal diffusion of heavy metals within CB-P and CB-M400, which occurred in three stages for the former and two stages for the latter. From the Weber-Morris model, q_t and $t^{1/2}$ plot are essential via the origin if the intra-particle is a rate-limiting step [11-15]. Therefore, the intra-particle diffusion of Pb (II) adsorption by CB-P and CB-M400 was not the rate-controlling step. The three-stage diffusion model is illustrated in the q_t and $t^{1/2}$ plot, in which the first part is attributed to boundary layer diffusion, the second to the intra-particle diffusion, and the third to the chemical reaction [12]. Because the pore size and volume of CB-M400 was less than in CB-P, intra-particle diffusion occurred simultaneously with film diffusion in the former. Accordingly, the boundary film diffusion should be assumed as the rate-limiting step of Pb (II) adsorption in both adsorbents.

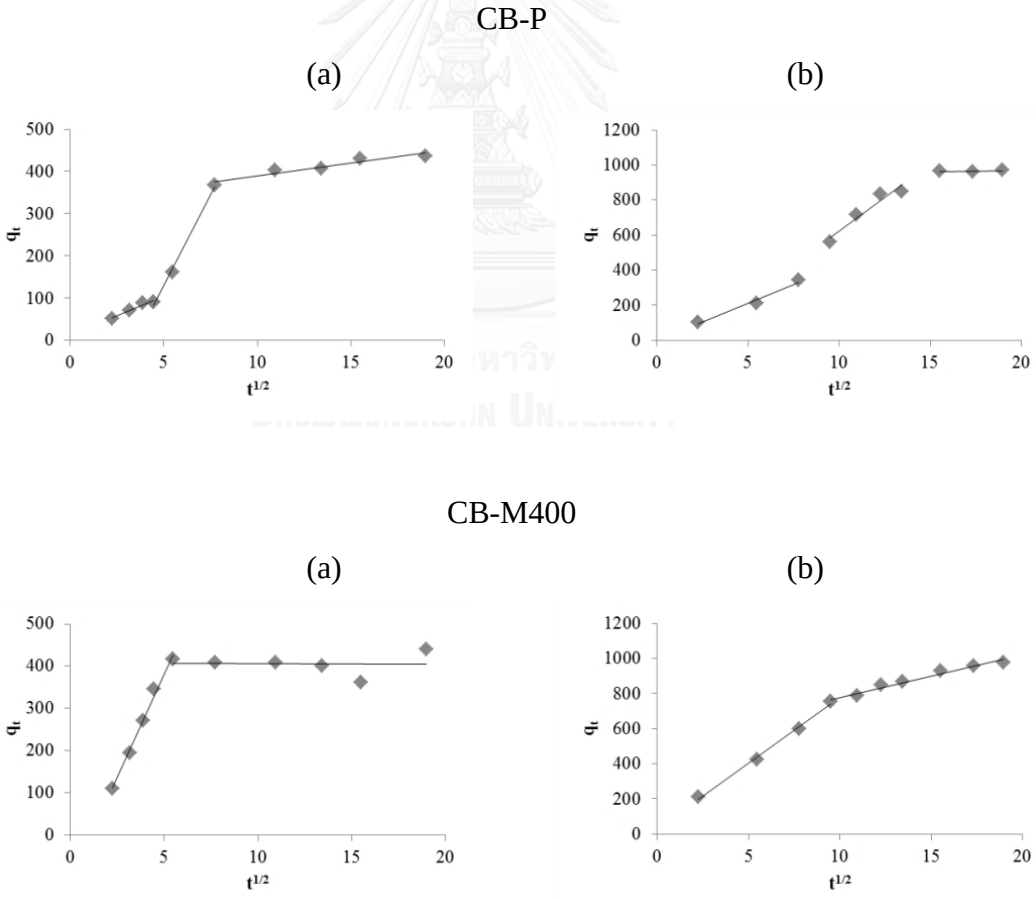

Figure 4.10 Intra-particle diffusion kinetics of Pb (II) onto CB-P and CB-M400, with initial concentrations of 100 mg/L (a) and 500 mg/L (b)

4.5 Adsorption interference

Figure 4.11 shows the adsorption capacity of CB-P and CB-M400 in a single Pb (II) system and a binary heavy metals system. When adjusted to pH 4.0, the concentration of Fe decreased by about 50 %. The overall adsorption capacity of CB-P and CB-M400 in both systems displayed an insignificantly different statistical trend with the equilibrium after 120 minutes. The capacity's changing rate from 5-120 minutes and the capacity in the equilibrium of CB-M400 in the single Pb (II) system were more valuable than those of CB-P. For the Pb (II) and Fe (II) binary heavy metals system, CB-P adsorbed Pb (II) at a higher rate and the adsorption capacity at the equilibrium was less than for the single Pb (II) system. For CB-M400, with the Pb (II) and Fe (II) system, adsorption rate at 5-45 minutes was similar to that for the single Pb (II) system; the Pb (II) take-up capacity at 60-360 minutes had variable changes to its value, according to the capacity at 360 minutes in the single Pb (II) system. When Pb (II) was combined with the Cr (III) system, the Pb (II) adsorption capacities of both CB-P and CB-M400 were constant, with a clearly lower value than for the single Pb (II) system.

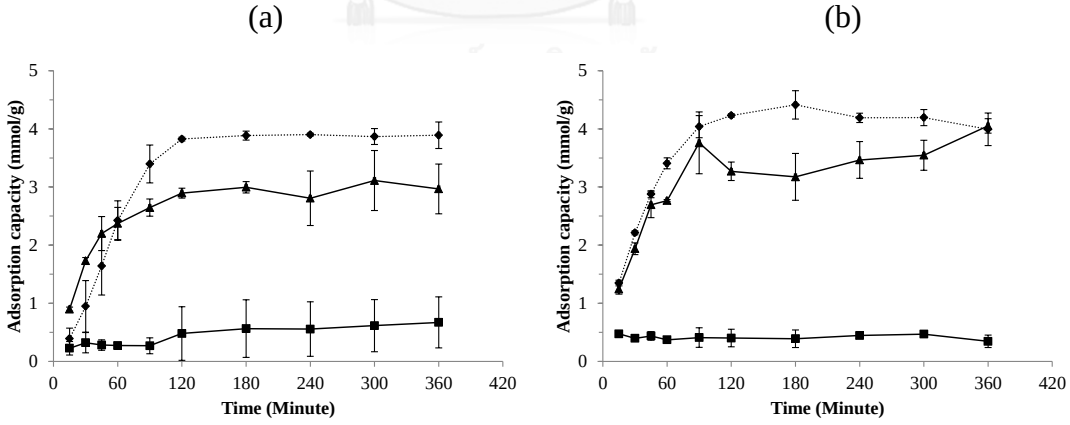

Figure 4.11 Pb (II) adsorption capacity of CB-P (a) and CB-M400 (b) in single Pb (II) system (●), Pb (II) + Fe (II) system (□), and Pb (II) + Cr (III) system (▲)

* Using synthetic wastewater Pb (II), Fe (II), and Cr (III) at an initial concentration of 1 mmol/L, a pH of 4.0, and an adsorbent dosage of 0.2 g/L, at 30 °C

Considering their equal heavy metals concentration and dose, the active binding sites were limited; the competitive ions adsorption was dependent on the ions' characteristics, the interaction of the heavy metal ions' behavior, and the ion selectivity of the active binding site [64-66]. The interaction of the multi-metal ions system was evaluated by the efficiency of removing the target metal in a multi-metals system, compared with a single system, which was considered as synergistic for increased efficiency, antagonistic for decreased efficiency, and as non-interactive behavior for constant efficiency [64]. The majority of the multi-heavy metals system adsorption study yielded a result of antagonistic interaction, whereby increased interference in ions caused a loss of efficiency in the removal of target ions [64-67].

Following this result, both Fe and Cr responded with antagonistic behavior in Pb (II) adsorption by CB-P and CB-M400. Due to Fe-OH precipitation, when adjusting the pH to 4.0, a low concentration of dissolved Fe was less effective in interfering in Pb (II) adsorption than Cr. Besides interference concentration, the oxidation state, complexation, and precipitation were also seen as interference factors.

The oxidation number of the heavy metals ion was referred to as ionic interaction with the active binding sites of adsorbents. As related with the solution pH by the oxidation reduction reaction, the oxidation states of Fe and Cr interacted in Pb (II) binding. The oxidation state of Fe (III) tends to have a greater binding affinity in the available site than Pb (II), so it may have blocked Pb (II) adsorption. Similarly, various oxidation states of Cr, including Cr (III) and Cr (VI), more strongly interrupted Pb (II) adsorption.

4.6 Battery wastewater

4.6.1 Wastewater composition

Based on the literature review and this study's analysis, the quality parameters of lead-acid battery manufacturing wastewater are shown in Table 4.7. The wastewater pH indicates an acid condition caused by H_2SO_4, leading to high total dissolved solids (TDS) from concentrate HSO_4^- and SO_4^{2-} ions. According to production process, the use of PbO, $PbSO_4$, and H_2SO_4 are the chief causes of Pb impurity in wastewater. Other contaminant ions may be deposited in wastewater by battery-plating paste composition and production unit corrosion [26].

Stability constants, solubility products, and the pH of the solution affect the species of heavy metal complexes and dissolve them [3, 4]. Suspended solids (SS) and dissolved solids were analyzed for heavy metals and other ions' composition. Most ions in wastewater occur as dissolved ions, excepting Pb and Zn. From our wastewater composition and heavy metals dissolution analysis, it can be explained that the complexation of Pb (II) and SO_4^{2-} in low pH forms less soluble solids of $PbSO_4$, which is also the case for particulates of Zn. However, soluble complexes of heavy metal ions that bind to NH_3 and Cl^- ligand may also possibly occur.

4.6.2 Wastewater treatment procedure

From the battery wastewater composition analysis, the TDS, pH, Pb, and Cr of the wastewater were over the industrial effluent standard limit; Ni, Mn, and Zn were lower than the standard limit, while Fe was at a high concentration without a standard limit. In basic concepts of wastewater treatment, the SS can be removed by sedimentation and filtration. Additionally, a coagulation-flocculation process may be used for increased particle sizes to accelerate sedimentation. Accordingly, wastewater pH, TDS, and dissolved heavy metals contamination are considered as parameters in the treatment process.

Table 4.8 Battery wastewater quality parameters with measured values and industrial effluent standard limits

Parameters	Value								Industrial effluent standard limit [68]
	[42]	[56]	[60]	[59]	[40]	This study			
						Dissolved	Particulate	Total	
pH	2.8-3.5	1.35-1.45	1.53-1.62	< 1	4.2	-	-	0.72 ± 0.02	5.0-9.0
SS (mg/L)	-	18.13	-	5397	-	-	-	67 ± 0.01	< 50
TDS (mg/L)	-	2227.47	-	55292	-	-	-	33362 ± 0.61	< 3.0
Pb (mg/L)	4.5	2.365	3.094	93.89	2.66	2.83 ± 0.01	30.37 ± 1.67	33.2	< 0.2
Ni (mg/L)	-	-	0.005	-	-	0.78 ± 0.01	-	0.78	< 1.0
Cu (mg/L)	-	-	0.027	-	-	0.093 ± 0.006	-	0.093	< 2.0
Total Cr (mg/L)	-	-	0.373	-	-	1.78 ± 0.02	-	1.78	< 0.25*
Zn (mg/L)	-	-	-	-	1.06	0.45 ± 0.12	2.38 ± 0.34	2.83	< 5.0
Mn (mg/L)	-	-	-	-	0.0284	1.48 ± 0.01	-	1.48	< 5.0
Cd (mg/L)	-	-	-	-	-	-	0.0001 ± 0.00002	0.0001	-
Co (mg/L)	-	-	-	-	-	0.0043 ± 0.004	-	0.0043	-
Fe (mg/L)	-	-	-	-	-	88.57 ± 2.99	0.27 ± 0.01	88.84	-
NH_4^+ (mg/L)	-	-	-	-	-	0.55 ± 0.04	-	0.55	-
SO_4^{2-} (mg/L)	100-200	-	-	-	-	28572 ± 0.52	17.49 ± 1.17	28590	-
Cl^- (mg/L)	30-50	-	-	-	-	3080 ± 0.22	-	3080	< 1.0
NO_3^- (mg/L)	2-พ.ค.	-	-	-	-	0.80 ± 0.13	-	0.8	-
PO_4^{3-} (mg/L)	-	-	-	-	-	0.19 ± 0.01	0.02 ± 0.002	0.21	-

* Standard value of Cr (VI)

The application of CB-P and CB-M400 in battery wastewater treatment was investigated using three treatments.

Treatment I: Dissolved battery wastewater was added to adsorbents.

Figure 4.12 shows the wastewater quality parameters after processing via treatment I, using standard limits. Overall, following treatment, the quality parameters were not significant for CB-P and CB-M400, excluding Ni. After the experiment, the parameters that exceeded the standards were slightly modified. In both the CB-P and CB-M400 experiments, the wastewater pH, TDS, and Pb were significantly changed from their initial values after treatment and slightly altered when using more adsorbents, but the value was not within the standard limit range. Mn and Zn were not clearly seen to slowly decrease, with no statistically significant difference from the initial concentration. Cr and Fe were unchanged, with a 95 % confidence interval. The Ni concentration was unchanged in the CB-P treatment, and slightly altered to less than the initial concentration in the CB-M400 assay.

The dissolution of $CaCO_3$ content in the adsorbents resulted in the CO_3^{2-} equilibrium and a subtle increase in the wastewater pH and discharged Ca^{2+} ions. The HSO_4^- and SO_4^{2-} equilibrium in the wastewater composition shifted to a state of having more SO_4^{2-} ions and enhanced metals-SO_4^{2-} complexation, which also had the effect of increasing the pH. Therefore, the formation of $PbSO_{4(s)}$ and $CaSO_{4(s)}$ may have reduced TDS, mainly due to HSO_4^- and SO_4^{2-}. For heavy metals removal, because of the $CaCO_3$ content dissolution in the acid solution, the other contents of the adsorbents played a function in heavy metals adsorption. The Pb removal was a special case, as it was significantly different due to enhanced SO_4^{2-} precipitation.

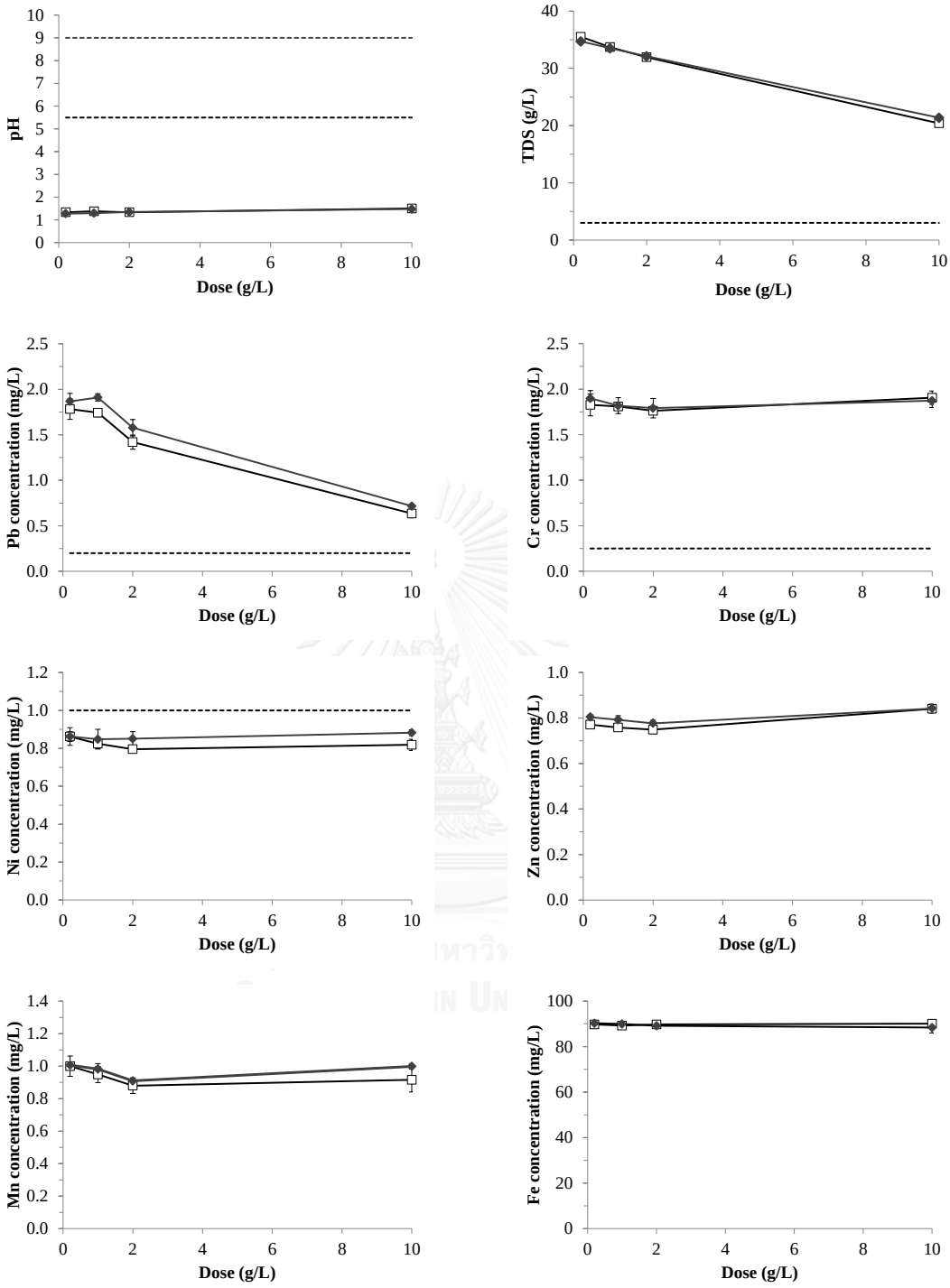

Figure 4.12 Industrial effluent standard limits (▪▪▪▪) and wastewater quality parameters (pH, TDS, Pb, Cr, Ni, Zn, Mn, and Fe) after processing using treatment I with CB-P (◆) and CB-M400 (□)

* Adsorbent dosage of 0.2-10.0 g/L, for 240 minutes at 30°C

Treatment II: Dissolved battery wastewater, with pH adjusted to 4.0 by NaOH, was added to adsorbents.

As illustrated in Figure 4.13, all heavy metals concentrations in the wastewater, with pH adjusted to 4.0 by NaOH, were significantly varied to a lower concentration than that seen in the initial wastewater, except Ni, which did not show a statistical difference. Figure 4.14 shows the wastewater quality after processing using treatment II within standard limits. After addition of the adsorbents, the wastewater's pH was increased within the standard range. The TDS was slightly enhanced from the wastewater pH of 4.0, which was still above the standard value. All heavy metals were shifted to below the standard limit. Overall, the parameters after treatment did not show significant results for either CB-P or CB-M400. Only the TDS in the CB-M400 treatment was slightly higher than in the CB-P treatment, with 95 % significance.

While adjusting the wastewater's pH to 4.0 using NaOH, some heavy metals formed solid complexes with SO_4^{2-} and OH^-, resulting in a clearly decreasing concentration of TDS (33.36 g/L to 13.58 g/L), Fe (88.57 mg/L to 5.06 mg/L), Cr (1.78 mg/L to 0.56 mg/L), and Pb (2.83 mg/L to 1.38 mg/L). After augmenting with CB-P and CB-M400, contaminated heavy metals were removed by CO_3^{2-} precipitation and adsorption on the adsorbents' surfaces. In addition, the Ca^{2+} from dissolved $CaCO_3$ content slightly induced an increase in the TDS. To be specific, it went over the standard TDS in the baseline of added soluble Na^+ ions, which were not removed by adsorbents.

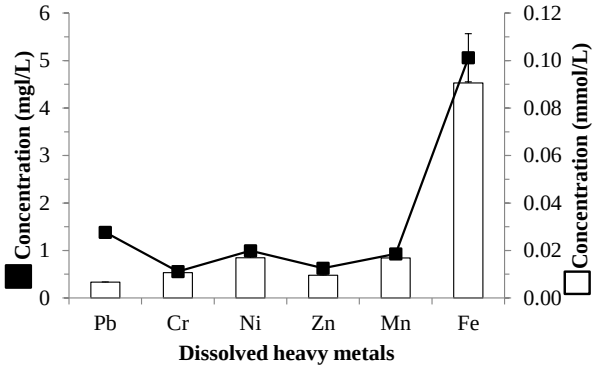

Figure 4.13 Concentration of heavy metals in dissolved battery wastewater with pH of 4.0 (adjusted by NaOH)

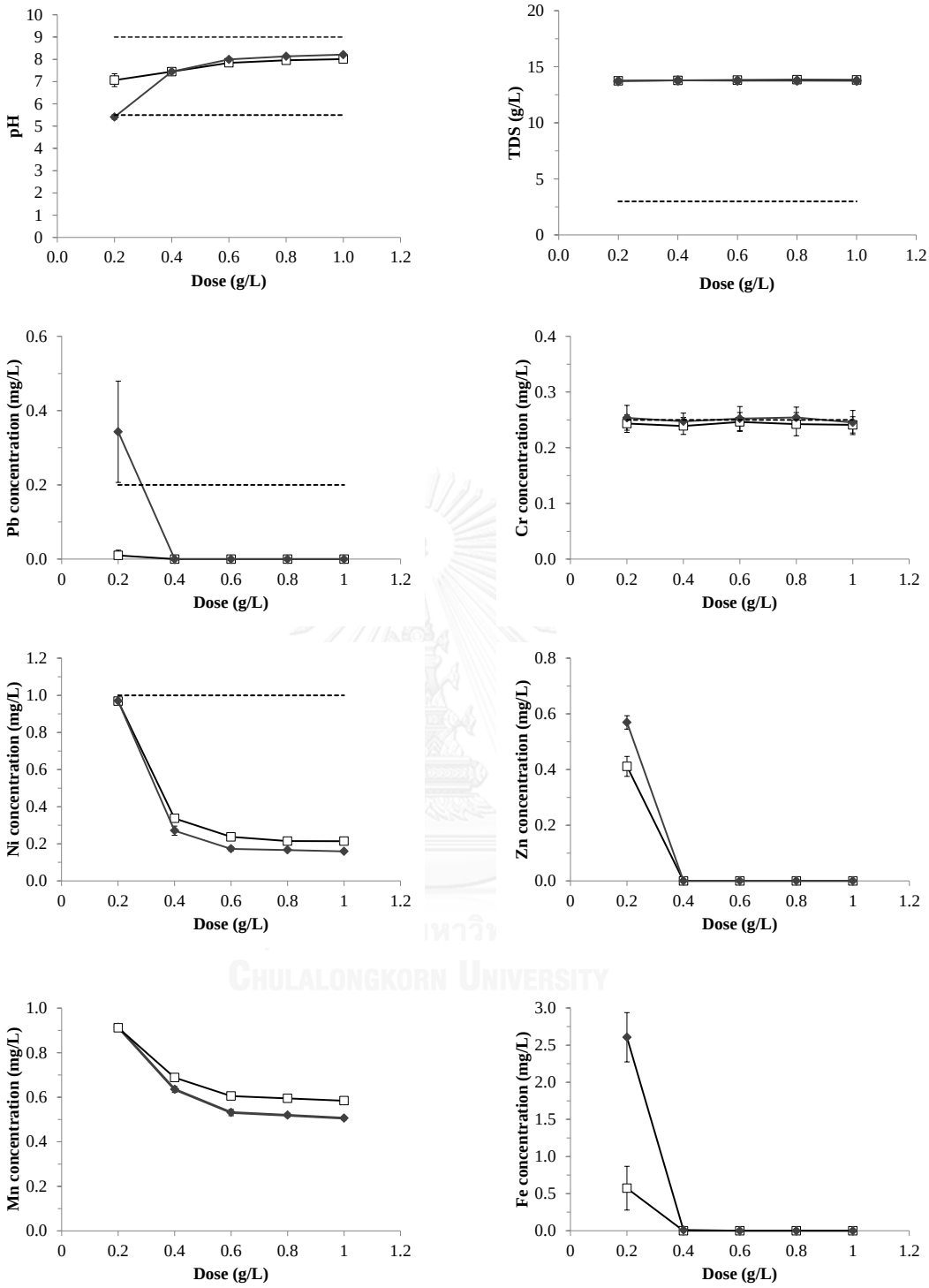

Figure 4.14 Industrial effluent standard limits (▪▪▪▪) and wastewater quality parameters (pH, TDS, Pb, Cr, Ni, Zn, Mn, and Fe) after processing using treatment II with CB-P (◆) and CB-M400 (□)

* Adsorbent dosage of 0.2-10.0 g/L, in wastewater with pH adjusted by NaOH, for 240 minutes at 30°C

Treatment II's results may well infer a specific ion removal and ion competition in heavy metals adsorption. We can assume that SO_4^{2-} was at a very low concentration, and its complexes had no effect on heavy metals adsorption. Because Fe represents the antagonistic behavior in Pb (II) adsorption, a high concentration of Fe in a multi-metals system allows more opportunity for its removal. Accordingly, contaminated Fe was adsorbed more than the other metals. These were Pb, Cr, Ni, Mn, and Zn, which were approximated as equivalent mole ratios; both adsorbents removed more Pb and Cr than Zn, Ni, and Mn.

Treatment III: Dissolved battery wastewater with $Ca(OH)_2$ pretreatment was added to CB-P, CB-M400, $Ca(OH)_2$, and $CaCO_3$.

$Ca(OH)_2$ pretreatment resulted in a reduction of TDS to the tune of 3.09-3.60 g/L and an increase in pH from 2.27-2.78. Figure 4.15 shows the wastewater quality parameters after processing using treatment III, within effluent standard limits. Overall, the parameters (pH, TDS, Pb, and Cr) were altered to the standard limit after the addition of CB-P, CB-M400, $Ca(OH)_2$, or $CaCO_3$ at 1.0 g/L. With all four, the wastewater's pH and concentrations of Pb and Zn after treatment were not different, with a significant level of 0.05. TDS, Cr, and Mn were not significant under $Ca(OH)_2$ and $CaCO_3$ treatment, which were at lower concentrations than CB-P and CB-M400. Only Ni, after treatment with $Ca(OH)_2$, was at a significantly lower concentration than other reagents.

The strong base chemical $Ca(OH)_2$, which was used in pretreatment, increased the wastewater's pH. Although its solubility was dependent on the solution's pH, and it was seen not to fully dissolve in water ($K_{sp} = 10^{-5.32}$), consisting of TDS, SO_4^{2-} was removed by $CaSO_4$ precipitation, which was less soluble ($K_{sp} = 10^{-4.85}$) [3, 4]. In the next step, CB-P, CB-M400, $CaCO_3$, and $Ca(OH)_2$ were augmented for the neutralization of wastewater pH, removal of heavy metals, and retention of SO_4^{2-}. Heavy metals precipitation by CO_3^{2-} was the reaction with CB-P, CB-M400, and $CaCO_3$, while OH^- precipitate appeared in $Ca(OH)_2$. However, heavy metals were ineffectively removed in a low concentration of reagents, because they contained $CaSO_4$ precipitate from the $Ca(OH)_2$ pretreatment, which may have interfered with the reaction.

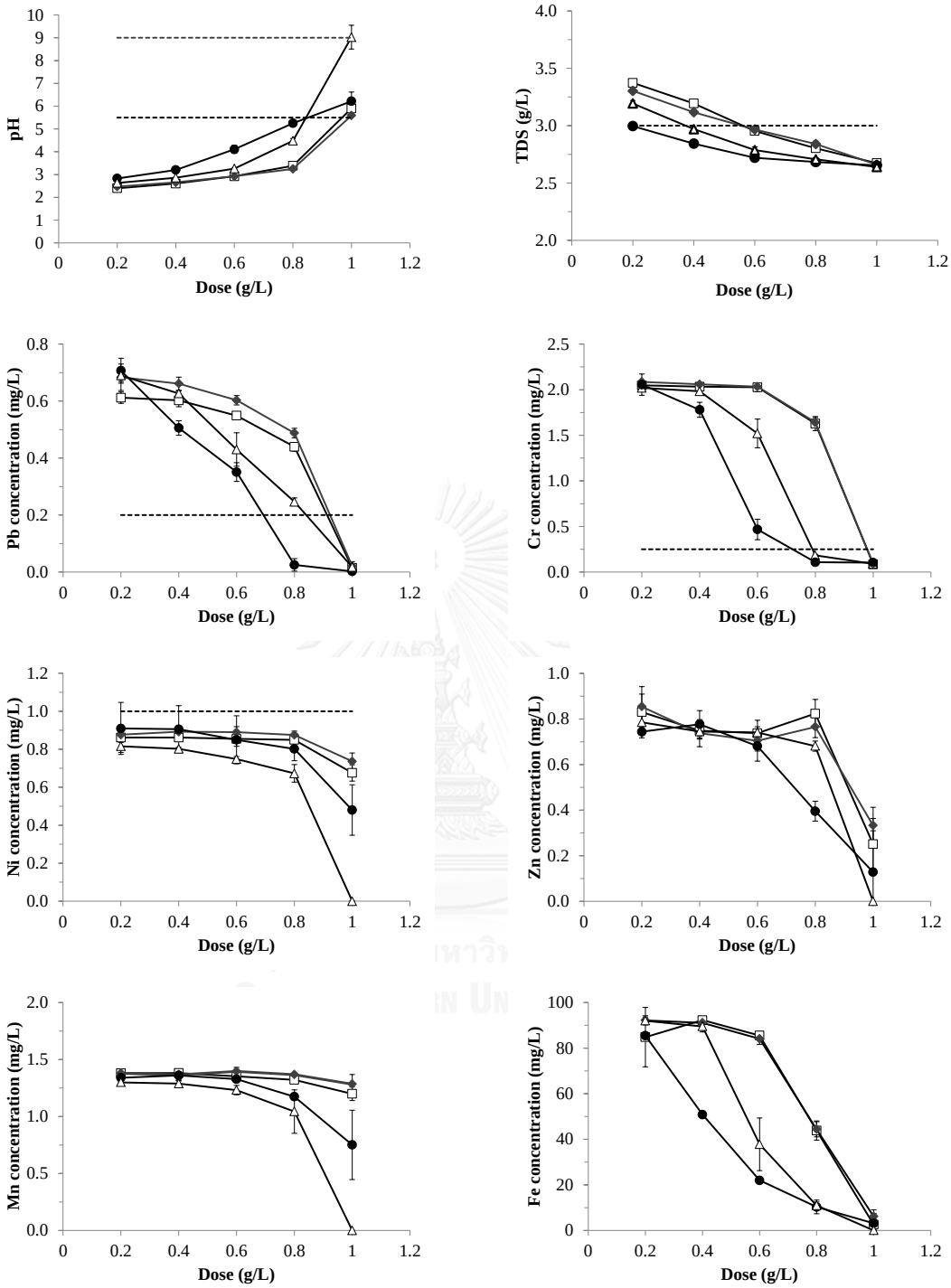

Figure 4.15 Industrial effluent standard limits (▪▪▪▪) and wastewater quality parameters (pH, TDS, Pb, Cr, Ni, Zn, Mn, and Fe) after processing using treatment III with CB-P (◆), CB-M400 (□), $CaCO_3$ (●), and $Ca(OH)_2$ (△)

* Reagent dosage of 0.2-1.0 g/L, wastewater added to $Ca(OH)_2$ at 16.46 g/L, for 240 minutes at 30°C

According to treatments I, II, and III, CB-P and CB-M400 have potential for application in battery manufacturing wastewater treatment, in the same way as NaOH, $CaCO_3$, and $Ca(OH)_2$. In order to choose the correct treatment, various factors including treated water quality, amount of sludge, sludge stability, and post-treatment for better quality, are considered necessary criteria.

Heavy metals precipitation and pH neutralization are widely used methods. NaOH is a basic chemical for conducting both of the above. As shown by the treatment II results, the use of NaOH to balance pH produces a stable value of TDS from dissolved Na^+ ions. To remove SO_4^{2-}, which is the main component of TDS, $Ca(OH)_2$ was used for the $CaSO_4$ precipitate. With reference to the effluent standard value of pH, which ranks between 5.5-9.0, due to the strong base behavior and solubility of $Ca(OH)_2$, not all soluble $Ca(OH)_2$ was a barrier to the control of the wastewater's pH. As presented by the treatment III results, with a slightly higher dose of $Ca(OH)_2$ (0.8 to 1.0 g/L), the wastewater's pH rapidly increased to 9.0 and posed a risk of exceeding the standard value if a greater dose was to be used. Meanwhile, a higher dose of CB-P, CB-M400, or $CaCO_3$ produced a slow increase in the pH, contributing to the pH resistance of the HCO_3^{2-} and CO_3^{2-} buffer.

The amount of sludge produced by the treatment process is a main concern in waste disposal and management. The quantity of chemicals expended in treatment can determine the volume of sludge produced. Treatment I involved the treatment of wastewater quality by CB-P and CB-M400; it is possible to improve this by adding a higher dose of adsorbent. Charge neutralization and heavy metals precipitation of $CaCO_3$, CB-P, and CB-M400 were the mechanisms of wastewater treatment, which resembled $Ca(OH)_2$, but due to $CaCO_3$'s molecular weight, the amount of dose to be used may be greater than that of $Ca(OH)_2$.

Discharged heavy metals from sludge, which depend on the stability of the heavy metals complex, are one of the key points in sludge management. As occurring in CB-P, CB-M400, and to a reasonable extent in $CaCO_3$, precipitate $Pb_3(CO_3)_2(OH)_2$ ($K_{sp} = 10^{-45.46}$) was more stable than in $Pb(OH)_2$ ($K_{sp} = 10^{-14.3}$) and $PbCO_3$ ($K_{sp} = 10^{-13.13}$) [3, 4]. The special consistency of $CaCO_3$, CB-P, and

CB-M400, namely the chitin and protein content in CB-P and fixed carbon content in CB-M400, increased the stability of Pb precipitate by Pb ions and the small-sized Pb precipitates' adsorption. In addition, heavy metals in leachate from sludge should be adsorbed by excess CB-P and CB-M400 adsorbents.

To treat wastewater, a combination of different methods was applied, such as increased removal efficiency by Fe (III) co-precipitation, enlarged precipitate size by coagulation-flocculation, and removal of precipitate sludge by sedimentation and sand filtration [27, 69]. As per previous studies [27, 70], advance techniques were developed for more effective wastewater treatment. Electrocoagulation, which used Fe and stainless steel rod electrodes with energy demands, produced more condensed heavy metals sludge than chemical precipitation, to the tune of 0.084-0.091 kg/m^3 [70]. As a result of the high TDS value, an ion exchange process was performed for the obtainment of TDS [27].

To respond to the demands of resource and waste management strategies, the use of renewable biological materials has been investigated to assess their performance in battery wastewater treatment [40, 42, 56, 59, 60]. As presented in this study, CB-P and CB-M400, as derived from cuttlebone, constitute an attractive alternative for heavy metals removal and wastewater treatment.

CHAPTER V
CONCLUSION AND FUTURE RESEARCH

5.1 Conclusion

The modification of cuttlebone as a biosorbent, namely cuttlebone powder (CB-P) and cuttlebone modified by carbonization at 400 ℃ (CB-M400), were investigated for their Pb (II) adsorption potential. The results of the adsorbents' characterization, study, and application for battery wastewater treatment are summarized as follows:

The crystalline of $CaCO_3$, of which aragonite and calcite are the main components, included 97.23 ± 0.10 % in CB-P and 99.59 ± 0.07 % in CB-M400. The observation of a corrugated and rough surface on CB-P and a smooth sheet on the surface of CB-M400 pointed to a higher specific surface area and porosity in CB-P. After Pb (II) adsorption, $PbCO_3$ and $Pb_3(CO_3)_2(OH)_2$ showed Pb precipitation by CO_3^{2-} and adsorption on the surface. The organic content of protein and chitin in CB-P and fixed carbon from the organic carbonization in CB-M400 support Pb (II) removal by the adsorption of Pb (II) and Pb precipitates.

For the removal of Pb (II) from synthetic wastewater, the overall capacity and efficiency of CB-P and CB-M400 were not significant under the same conditions. $CaCO_3$ dissolution, functional group dissociation, and the amount of available active sites were influenced by the solution's pH, the adsorbent dose, and the initial Pb (II) concentration. By mixing for 240 minutes at 100 rpm at 30°C, Pb (II) removal by CB-P and CB-M400 was optimum at a pH of 4.0 and with an adsorbent dose of 0.2 g/L. As fixed with the Langmuir isotherm, the adsorption equilibrium was monolayer adsorption, which evaluated a maximum capacity of 860.57 mg/g for CB-P and 1573.56 mg/g for CB-M400. In the kinetic study, Pb (II) removal from initial concentrations of 100 and 500 mg/L found the equilibrium in 240 minutes. The reaction rate constant of CB-M400, as calculated from a suitable pseudo-second-order reaction, was greater than that of CB-P; therefore, film diffusion on the adsorbents' surface was the rate-controlling step. Contaminated Fe (II) or Cr (III) in

the Pb (II) solution of the binary heavy metals system interfered with Pb (II) adsorption by competitive adsorption; this had more impact with Cr (III).

The application of CB-P and CB-M400 in lead-acid battery manufacturing wastewater treatment, which was combined with $Ca(OH)_2$ pretreatment, was successful in pH neutralization and the removal of total dissolved solids (TDS) and heavy metals (Pb, Cr, Ni, Zn, Mn, and Fe), in the same way as $CaCO_3$ and $Ca(OH)_2$. According to the results, cuttlebone can be modified as an alternative option for wastewater treatment, which can form a guideline for the utilization of cuttlefish waste products.

5.2 Future research

5.2.1 Explain heavy metals' adsorption in variable concentrations of multi-metal systems and other contained compounds systems.

5.2.2 Design a more effective modified cuttlebone adsorbent.

5.2.3 Study the quality and quantity of sludge from wastewater treatment using cuttlebone for sludge management.

5.2.4 Assess the operating treatment system and economical possibility of using cuttlebone in wastewater treatment.

REFERENCES

[1] Fu, F., Wang, Q. 2011. Removal of heavy metal ion from wastewater: A review. Journal of Environmental Management. 92: 407-418.

[2] Arbabi, M., Hemati, S., Amiri, M. 2015. Removal of lead ions from industrial wastewater: a review of removal methods. International Journal of Epidemiologic Research. 2: 105-109.

[3] Benjamin, M. M. 2002. Water chemistry. 1 ed. Singapore: McGraw-Hill.

[4] Snoeyink, V. L., Jenkins, D. 1980. Water chemistry. New York: John Willy & sons.

[5] Sawyer, C. N., McCarty, P. L., Parkin, G. F. 1994. Chemistry for environmental engineering. 4 ed. Singapore: McGraw-Hill.

[6] Mudhoo, A., Garg, V. K., Wang, S. 2011. Removal of heavy metals by biosorption. Environmental Chemistry Letters. 10: 109-117.

[7] Febrianto, J., Kosasih, A. N., Sunarso, J., Ju, Y. H., Indraswati, N., Ismadji, S. 2009. Equilibrium and kinetic studies in adsorption of heavy metals using biosorbent: A summary of recent studies. Journal of Hazardous Materials. 162: 616-645.

[8] Foo, K. Y., Hameed, B. H. 2010. Insights into the modeling of adsorption isotherm systems. Chemical Engineering Journal. 156: 2-10.

[9] Kılıç, M., Kırbıyık, Ç., Çepelioğullar, Ö., Pütün, A. E. 2013. Adsorption of heavy metal ions from aqueous solutions by bio-char, a by-product of pyrolysis. Applied Surface Science. 283: 856-862.

[10] Azizian, S. 2004. Kinetic models of sorption: A theoretical analysis. Journal of Colloid and Interface Science. 276: 47-52.

[11] Qiu, H., Lv, L., Pan, B., Zhang, Q., Zhang, W., Zhang, Q. 2009. Critical review in adsorption kinetic models. Journal of Zhejiang University SCIENCE A. 10: 716-724.

[12] Lazaridis, N. K., Asouhidou, D. D. 2003. Kinetics of sorptive removal of chromium(VI) from aqueous solutions by calcined Mg–Al–CO3 hydrotalcite. Water Research. 37: 2875-2882.

[13] Hu, X. J., et al. 2011. Adsorption of chromium (VI) by ethylenediamine-modified cross-linked magnetic chitosan resin: isotherms, kinetics and thermodynamics. Journal of Hazardous Materials. 185: 306-314.

[14] Li, Q., Zhai, J., Zhang, W., Wang, M., Zhou, J. 2007. Kinetic studies of adsorption of Pb(II), Cr(III) and Cu(II) from aqueous solution by sawdust and modified peanut husk. Journal of Hazardous Materials. 141: 163-167.

[15] Argun, M. E., Dursun, S., Ozdemir, C., Karatas, M. 2007. Heavy metal adsorption by modified oak sawdust: thermodynamics and kinetics. Journal of Hazardous Materials. 141: 77-85.

[16] Denton, E. J., Gilpin-Brown, J. B. 1959. Buoyancy of the cuttlefish. Nature. 183: 1330-1331.

[17] Birchall, J. D., Thomas, N. L. 1983. On the architecture and function of cuttlefish bone. Journal of Materials Science. 18: 2081-2086.

[18] Abdou, E. S., Nagy, K. S., Elsabee, M. Z. 2008. Extraction and characterization of chitin and chitosan from local sources. Bioresource Technology. 99: 1359-136767.

[19] Sagheer, F. A. A., Al-Sughayer, M. A., Muslim, S., Elsabee, M. Z. 2009. Extraction and characterization of chitin and chitosan from marine sources in Arabian Gulf. Carbohydrate Polymers. 77: 410-419.

[20] Florek, M., et al. 2009. Complementary microstructural and chemical analyses of *Sepia officinalis* endoskeleton. Materials Science and Engineering: C. 29: 1220-1226.

[21] Klungsuwan, P. 2010.Mechanical propoties of cuttlebone reinforced natural rubber composites. Program in petrochemistry and polymer science, Faculty of Science, Chulalongkorn University.

[22] Cadman, J., Zhou, S., Chen, Y., Li, Q. 2012. Cuttlebone: Characterisation, application and development of biomimetic materials. Journal of Bionic Engineering. 9: 367-376.

[23] Li, Y. Z., et al. 2010. Characterization of metal removal by os sepiae of *Sepiella maindroni* Rochebrune from aqueous solutions. Journal of Hazardous Materials. 179: 266-275.

[24] Sandesh, K., Suresh Kumar, R., JagadeeshBabu, P. E. 2013. Rapid removal of cobalt (II) from aqueous solution using cuttlefish bones; equilibrium, kinetics, and thermodynamic study. Asia-Pacific Journal of Chemical Engineering. 8: 144-153.

[25] Ben Nasr, A., Walha, K., Charcosset, C., Ben Amar, R. 2011. Removal of fluoride ions using cuttlefish bones. Journal of Fluorine Chemistry. 132: 57-62.

[26] Dahodwalla, H., Herat, S. 2000. Cleaner production options for lead-acid battery manufacturing industry. Journal of Cleaner Production. 8: 133-142.

[27] Uddin, J., Mondal, P. K., Rahman, A., Lemon, H. R. 2013. An approach to reduce waste in lead acid battery industries. Global Journal of Researches in Engineering. 13: 16-22.

[28] Marani, D., Macchi, G., Pagand, M. 1995. Lead precipitation in the presence of sulphate and carbonate: Testing of thermodynamic predictions. Water Research. 24: 1085-1092.

[29] Macchi, G., Marani, D., Pagand, M., Bagnuolo, G. 1996. A bench study on lead removal from battery manufacturing wastewater by carbonate precipitation. Water Research. 30: 3032-3036.

[30] Matlock, M. M., Howerton, B. S., Atwood, D. A. 2002. Chemical precipitation of lead from lead battery recycling plant wastewater. Industrial & Engineering Chemistry Research. 41: 1579-1582.

[31] Ibrahim, W. M. 2011. Biosorption of heavy metal ions from aqueous solution by red macroalgae. Journal of Hazardous Materials. 192: 1827-1835.

[32] Bulgariu, D., Bulgariu, L. 2012. Equilibrium and kinetics studies of heavy metal ions biosorption on green algae waste biomass. Bioresource Technology. 103: 489-493.

[33] Yalcin, S., Sezer, S., Apak, R. 2012. Characterization and lead (II), cadmium (II), nickel (II) biosorption of dried marine brown macro algae *Cystoseira barbata*. Environmental science and pollution research international. 19: 3118-3125.

[34] Davis, T. A., Volesky, B., Mucci, A. 2003. A review of the biochemistry of heavy metal biosorption by brown algae. Water Research. 37: 4311-4330.
[35] Wang, J., Chen, C. 2009. Biosorbents for heavy metals removal and their future. Biotechnology Advances. 27: 195-226.
[36] Deng, P. Y., Liu, W., Zeng, B. Q., Qiu, Y. K., Li, L. S. 2013. Sorption of heavy metals from aqueous solution by dehydrated powders of aquatic plants. International Journal of Environmental Science and Technology. 10: 559-566.
[37] Tang, Y., Chen, L., Wei, X., Yao, Q., Li, T. 2013. Removal of lead ions from aqueous solution by the dried aquatic plant, *Lemna perpusilla* Torr. Journal of Hazardous Materials. 244-245: 603-612.
[38] Anwar, J., Shafique, U., Waheed uz, Z., Salman, M., Dar, A., Anwar, S. 2010. Removal of Pb (II) and Cd (II) from water by adsorption on peels of banana. Bioresource Technology. 101: 1752-1755.
[39] Taşar, Ş., Kaya, F., Özer, A. 2014. Biosorption of lead(II) ions from aqueous solution by peanut shells: Equilibrium, thermodynamic and kinetic studies. Journal of Environmental Chemical Engineering. 2: 1018-1026.
[40] Prado, A. G. S., et al. 2010. Thermodynamic aspects of the Pb adsorption using Brazilian sawdust samples: Removal of metal ions from battery industry wastewater. Chemical Engineering Journal. 160: 549-555.
[41] Wan Ngah, W. S., Hanafiah, M. A. 2008. Removal of heavy metal ions from wastewater by chemically modified plant wastes as adsorbents: a review. Bioresource Technology. 99: 3935-3948.
[42] Noeline, B. F., Manohar, D. M., Anirudhan, T. S. 2005. Kinetic and equilibrium modelling of lead (II) sorption from water and wastewater by polymerized banana stem in a batch reactor. Separation and Purification Technology. 45: 131-140.
[43] Sud, D., Mahajan, G., Kaur, M. P. 2008. Agricultural waste material as potential adsorbent for sequestering heavy metal ions from aqueous solutions - a review. Bioresource Technology. 99: 6017-6027.
[44] Demirbas, A. 2008. Heavy metal adsorption onto agro-based waste materials: A review. Journal of Hazardous Materials. 157: 220-229.
[45] Chen, X., et al. 2011. Adsorption of copper and zinc by biochars produced from pyrolysis of hardwood and corn straw in aqueous solution. Bioresource Technology. 102: 8877-8884.
[46] Komnitsas, K., Zaharaki, D., Bartzas, G., Kaliakatsou, G., Kritikaki, A. 2014. Efficiency of pecan shells and sawdust biochar on Pb and Cu adsorption. Desalination and Water Treatment. 57: 3237-3246.
[47] Liu, Z., Zhang, F. S. 2009. Removal of lead from water using biochars prepared from hydrothermal liquefaction of biomass. Journal of Hazardous Materials. 167: 933-939.
[48] Demirbas, A., Arin, G. 2002. An overview of biomass pyrolysis. Energy Sources. 24: 471-482.
[49] Lee, M., Park, J. M., Yang, J. 1997. Micro precipitation of lead on the surface of crab shell particles. Process Biochemistry. 32: 671-677.
[50] An, H. K., Park, B. Y., Kim, D. S. 2001. Crab shell for the removal of heavy metals from aqueous solution. Water Research. 35: 3551-3556.

[51] Vijayaraghavan, K., Palanivelu, K., Velan, M. 2006. Biosorption of copper (II) and cobalt (II) from aqueous solutions by crab shell particles. Bioresource Technology. 97: 1411-1419.

[52] Vijayaraghavan, K., Winnie, H. Y. N., Balasubramanian, R. 2011. Biosorption characteristics of crab shell particles for the removal of manganese (II) and zinc (II) from aqueous solutions. Desalination. 266: 195-200.

[53] Ahmad, M., et al. 2012. Eggshell and coral wastes as low cost sorbents for the removal of Pb^{2+}, Cd^{2+} and Cu^{2+} from aqueous solutions. Journal of Industrial and Engineering Chemistry. 18: 198-204.

[54] Vijayaraghavan, K., Joshi, U. M. 2013. Chicken eggshells remove Pb (II) ions from synthetic wastewater. Environmental Engineering Science. 30: 67-73.

[55] Soares, M. A. R., Marto, S., Quina, M. J., Gando-Ferreira, L., Quinta-Ferreira, R. 2016. Evaluation of eggshell-rich compost as biosorbent for removal of Pb (II) from aqueous solutions. Water, Air, & Soil Pollution. 227.

[56] Arunlertaree, C., Kaewsomboon, W., Kumsopa, A., Pokethitiyook, P., Panyawathanakit, P. 2007. Removal of lead from battery manufacturing wastewater by egg shell. Songklanakarin Journal of Science and Technology. 29: 858-868.

[57] Du, Y., Lian, F., Zhu, L. 2011. Biosorption of divalent Pb, Cd and Zn on aragonite and calcite mollusk shells. Environmental Pollution. 159: 1763-1768.

[58] Ramalingam, S., Parthiban, L., Rangasamy, P. 2014. Biosorption modeling with multilayer perceptron for removal of lead and zinc ions using crab shell particles. Arabian Journal for Science and Engineering. 39: 8465-8475.

[59] Chauhan, D., Sankararamakrishnan, N. 2008. Highly enhanced adsorption for decontamination of lead ions from battery wastewaters using chitosan functionalized with xanthate. Bioresource Technology. 99: 9021-9024.

[60] Bahadir, T., Bakan, G., Altas, L., Buyukgungor, H. 2007. The investigation of lead removal by biosorption: An application at storage battery industry wastewaters. Enzyme and Microbial Technology. 41: 98-102.

[61] Huang, C. K. a. K., P.F. 1960. Infrared study of the carbonate minerals. The American Mineralogist. 45: 311-324.

[62] Li, H., Jin, D., Li, R., Li, X. 2015. Structural and mechanical characterization of thermally treated conch shells. JOM. 67: 720-725.

[63] Sazanov, Y. N., et al. 2004. Carbonization of polyacrylonitrile composites with nitrogen-containing cellulose derivatives. Russian Journal of Applied Chemistry. 77: 639-644.

[64] Jain, M., Garg, V. K., Kadirvelu, K., Sillanpää, M. 2015. Adsorption of heavy metals from multi-metal aqueous solution by sunflower plant biomass-based carbons. International Journal of Environmental Science and Technology. 13: 493-500.

[65] Šćiban, M. B., Klašnja, M. T., Antov, M. G. 2011. Study of the biosorption of different heavy metal ions onto Kraft lignin. Ecological Engineering. 37: 2092-2095.

[66] Lee, Y. C., Chang, S. P. 2011. The biosorption of heavy metals from aqueous solution by Spirogyra and Cladophora filamentous macroalgae. Bioresource Technology. 102: 5297-5304.

[67] Figueira, M. M., Volesky, B., Ciminelli, V. S. T. 1997. Assessment of interference in biosorption of a heavy metal. Biotechnology and Bioengineering. 54: 344-350.

[68] Ministry of Science, Technology and Environment. 1996. Notification the Ministry of Science, Technology and Environment, No. 3, B.E.2539. under the Enhancement and Conservation of the National Environmental Quality Act B.E.2535. Royal Government Gazette: 113 part 13 D.

[69] Macchi, G., Pagand, M., Santor, M., Tiravanti, G. 1993. Battery industry wastewater: Pb removal and produced sludge. Water Research. 27: 1511-1518.

[70] Mansoorian, H. J., Mahvi, A. H., Jafari, A. J. 2014. Removal of lead and zinc from battery industry wastewater using electrocoagulation process: Influence of direct and alternating current by using iron and stainless steel rod electrodes. Separation and Purification Technology. 135: 165-175.

APPENDIX

APPENDIX A

XRD intensity pattern of adsorbents with aragonite, calcite, sodium chloride, lead carbonate and lead carbon hydrogen oxide intensity pattern

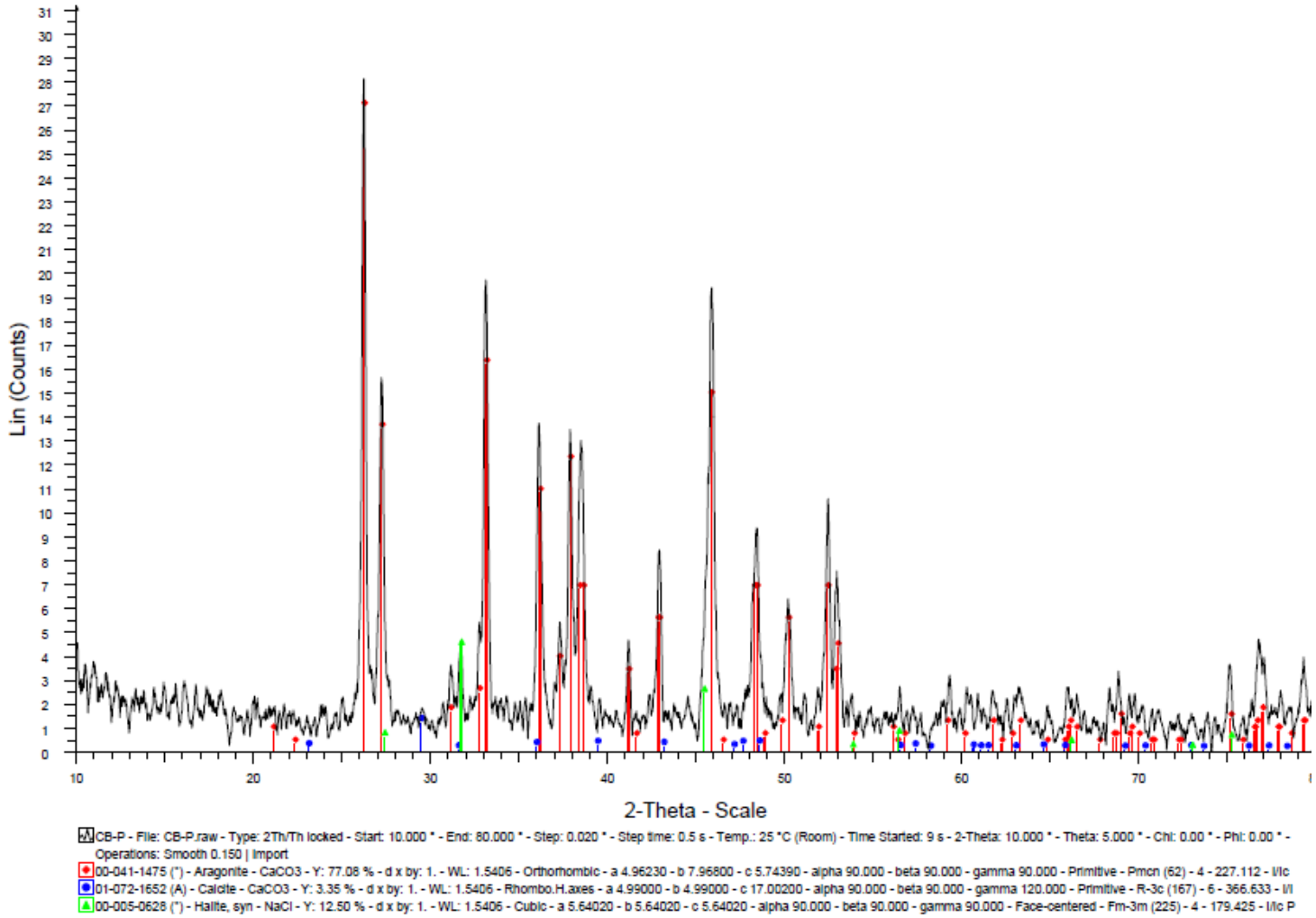

Figure A-1 XRD pattern of CB-P before Pb adsorption

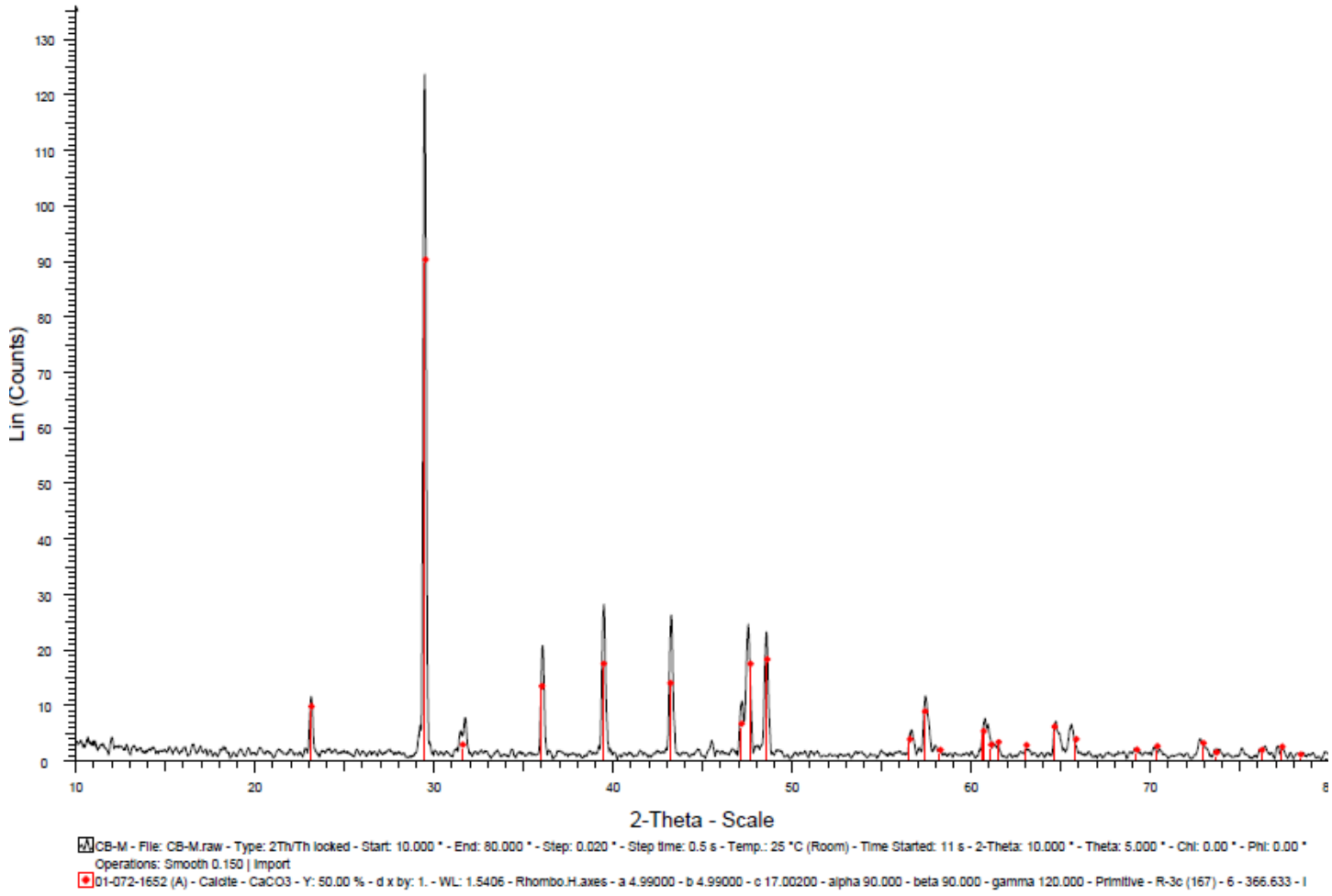

Figure A-2 XRD pattern of CB-M400 before Pb adsorption

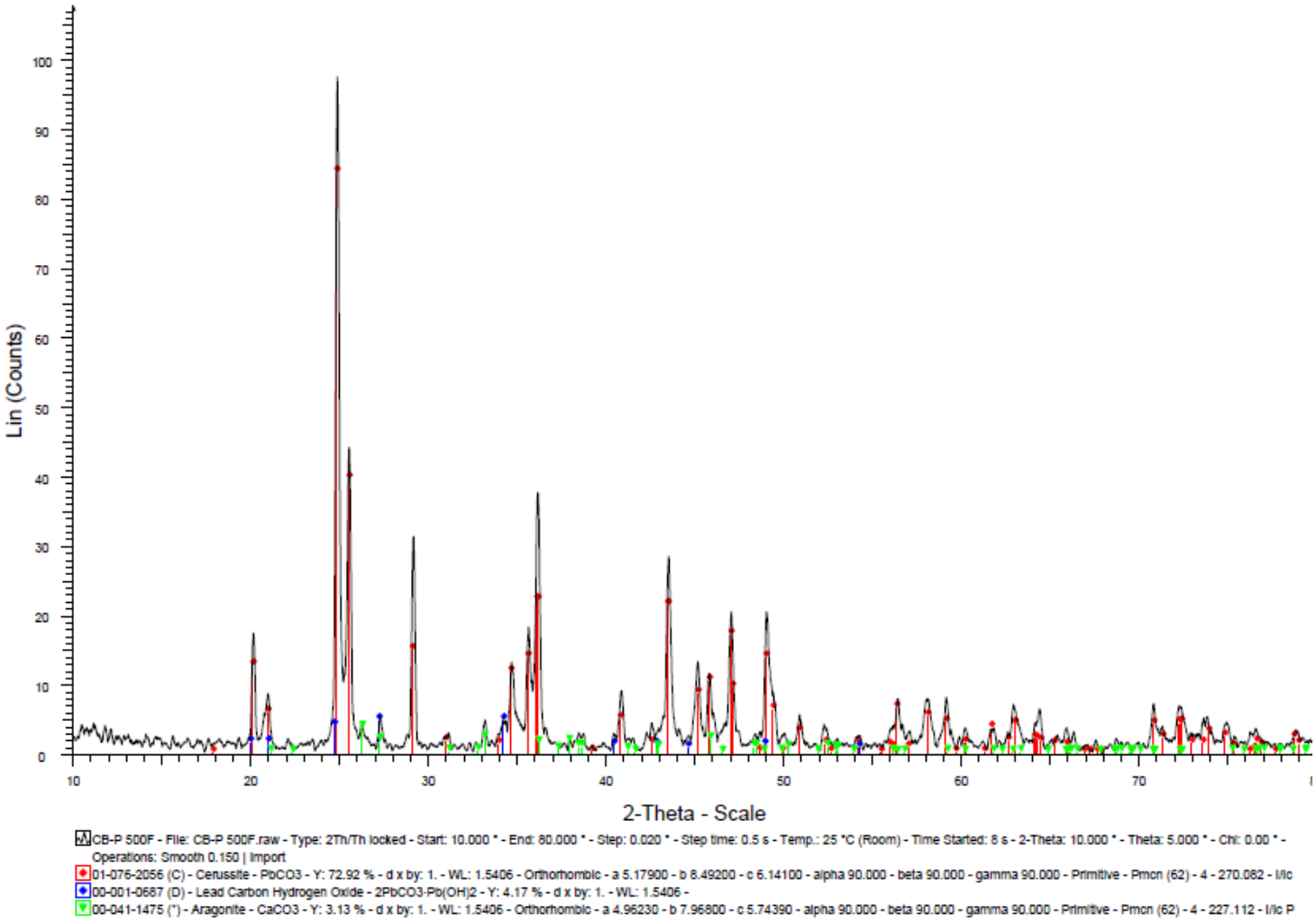

Figure A-3 XRD pattern of CB-P after Pb adsorption

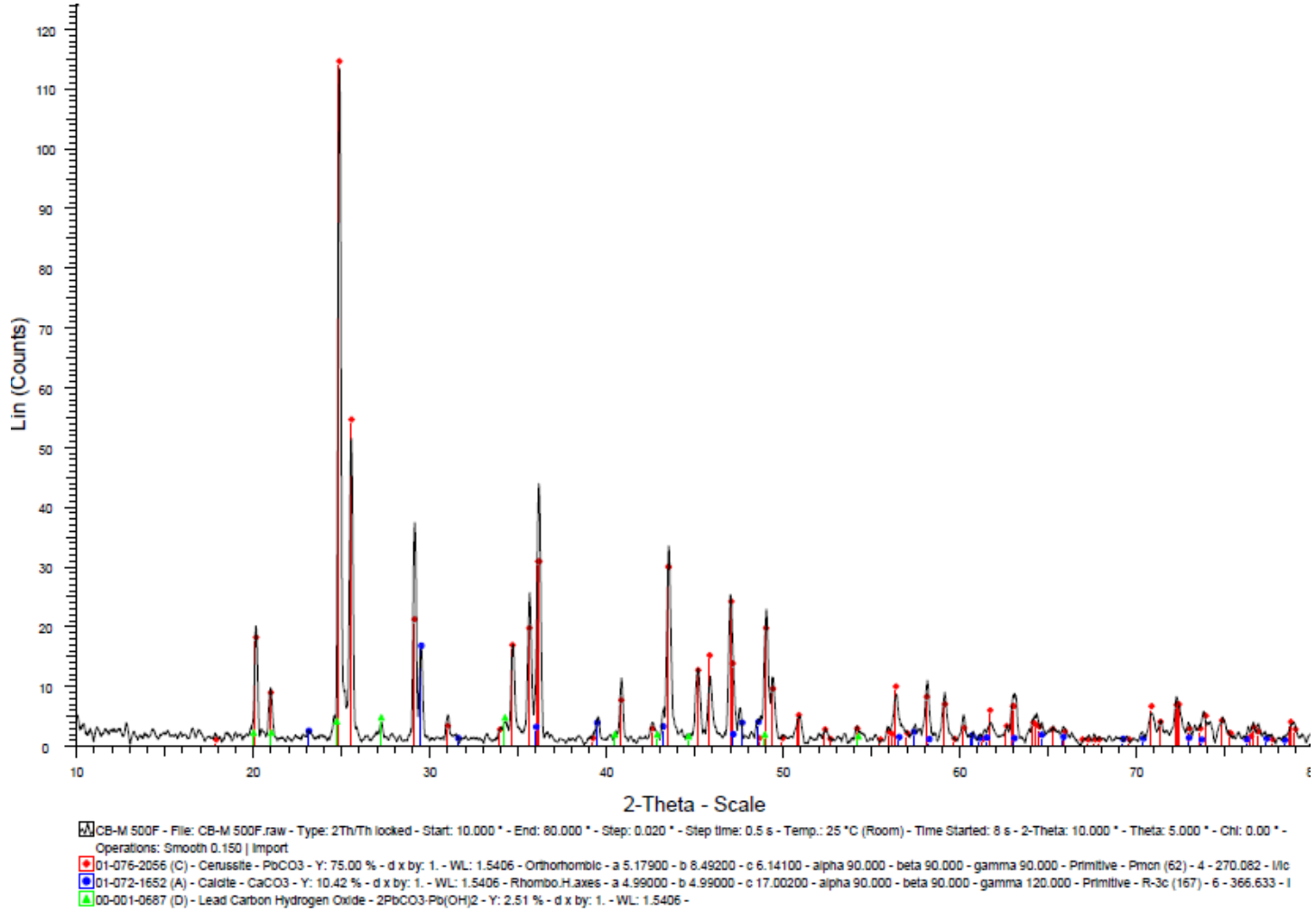

Figure A-4 CB-M400 after Pb adsorption

APPENDIX B

Effect of initials pH data and statistical analysis

Table B.1 One-way ANOVA of capacity and efficiency between group CB-P and CB-M400 in effect of initial pH study

		Sum of Squares	df	Mean Square	F	Sig.
Capacity	Between Groups	420.280	1	420.280	.002	.962
	Within Groups	5053940.915	28	180497.890		
	Total	5054361.195	29			
Efficiency	Between Groups	145.161	1	145.161	.075	.786
	Within Groups	54056.590	28	1930.592		
	Total	54201.751	29			

Table B.2 Pb (II) adsorption capacity and efficiency of CB-P and CB-M400 in effect of initial pH study with statistic significant between pH

pH	Capacity (mg/g)		Efficiency (mg/g)	
	CB-P	CB-M400	CB-P	CB-M400
1.0	12.99^{A}	88.12^{A}	1.29^{A}	9.12^{A}
2.0	17.60^{A}	123.25^{A}	1.74^{A}	13.40^{A}
3.0	772.64^{B}	680.05^{B}	73.62^{B}	74.03^{B}
4.0	969.75^{C}	933.30^{C}	97.07^{C}	99.27^{C}
5.0	987.60^{C}	898.59^{C}	99.51^{C}	99.42^{C}

* ^{A}, ^{B}, ^{C} and ^{D} show statistic significant with 95 % confidence interval

APPENDIX C

Effect of adsorbent dose and Pb (II) initials concentration data and statistical analysis

Table C.1 One-way ANOVA of capacity and efficiency between group CB-P and CB-M400 in effect of adsorbent dose and Pb (II) initial concentration study

		Sum of Squares	df	Mean Square	F	Sig.
Capacity	Between Groups	662708.216	1	662708.216	2.699	.103
	Within Groups	36340693.706	148	245545.228		
	Total	37003401.923	149			
Efficiency	Between Groups	1097.557	1	1097.557	1.208	.273
	Within Groups	134423.051	148	908.264		
	Total	135520.609	149			

Table C.2 One-way ANOVA of capacity and efficiency in each concentration between group CB-P (a) and CB-M400 (b)

			Sum of Squares	df	Mean Square	F	Sig.
Capacity	10 mg/L	Between Groups	755.337	1	755.337	2.384	.134
		Within Groups	8869.994	28	316.786		
		Total	9625.331	29			
	100 mg/L	Between Groups	126.702	1	126.702	.002	.968
		Within Groups	2189253.772	28	78187.635		
		Total	2189380.474	29			
	250 mg/L	Between Groups	1385.362	1	1385.362	.016	.901
		Within Groups	2469159.422	28	88184.265		
		Total	2470544.783	29			
	500 mg/L	Between Groups	31965.378	1	31965.378	.670	.420
		Within Groups	1335206.705	28	47685.954		
		Total	1367172.083	29			
	1000 mg/L	Between Groups	2626122.551	1	2626122.551	105.067	.000
		Within Groups	699854.475	28	24994.803		
		Total	3325977.026	29			
Efficiency	10 mg/L	Between Groups	.002	1	.002	1.000	.326
		Within Groups	.069	28	.002		
		Total	.071	29			
	100 mg/L	Between Groups	.001	1	.001	1.000	.326
		Within Groups	.033	28	.001		
		Total	.035	29			
	250 mg/L	Between Groups	35.642	1	35.642	.064	.802
		Within Groups	15495.219	28	553.401		
		Total	15530.862	29			
	500 mg/L	Between Groups	317.498	1	317.498	.398	.533
		Within Groups	22326.154	28	797.363		
		Total	22643.652	29			
	1000 mg/L	Between Groups	2520.737	1	2520.737	4.350	.046
		Within Groups	16224.853	28	579.459		
		Total	18745.590	29			

Table C.3 Pb (II) adsorption capacity and efficiency of adsorbent dose of CB-P (a) and CB-M400 (b) with statistic significant between adsorbent doses in each concentration

a)

Dose	Capacity (mg/g)					Efficiency (%)				
	10 mg/L	100 mg/L	250 mg/L	500 mg/L	1000 mg/L	10 mg/L	100 mg/L	250 mg/L	500 mg/L	1000 mg/L
0.1	66.35^{A}	871.79^{A}	830.61^{A}	1082.60^{A}	825.60^{A}	100.00^{A}	100.00^{A}	37.40^{A}	20.02^{A}	8.07^{A}
0.2	32.52^{B}	444.50^{B}	1046.73^{B}	1178.23^{A}	937.34^{A}	100.00^{A}	100.00^{A}	94.33^{B}	43.68^{B}	17.96^{B}
0.3	21.85^{C}	293.90^{C}	740.49^{A}	1150.75^{A}	932.43^{A}	99.91^{A}	99.94^{A}	99.99^{B}	64.41^{C}	26.88^{C}
0.5	13.17^{D}	175.70^{D}	444.40^{C}	868.10^{B}	954.27^{A}	100.00^{A}	100.00^{A}	99.99^{B}	80.60^{D}	45.85^{D}
0.7	9.45^{E}	126.22^{E}	316.40^{C}	730.90^{B}	908.58^{A}	100.00^{A}	100.00^{A}	99.99^{B}	94.85^{E}	60.49^{E}

b)

Dose	Capacity (mg/g)					Efficiency (%)				
	10 mg/L	100 mg/L	250 mg/L	500 mg/L	1000 mg/L	10 mg/L	100 mg/L	250 mg/L	500 mg/L	1000 mg/L
0.1	42.72^{A}	883.96^{A}	1006.43^{A}	1225.59^{A}	1772.87^{A}	100.00^{A}	100.00^{A}	48.37^{A}	24.03^{A}	17.25^{A}
0.2	21.35^{B}	444.53^{B}	1011.07^{A}	$1330.65^{A,\#}$	$1564.41^{A,\#}$	100.00^{A}	100.00^{A}	94.73^{B}	52.48^{B}	31.05^{B}
0.3	14.42^{C}	297.91^{C}	708.30^{B}	$1133.32^{B,\#}$	$1485.60^{B,\#}$	100.00^{A}	100.00^{A}	99.53^{C}	67.70^{C}	43.32^{C}
0.5	8.56^{D}	178.46^{D}	419.25^{C}	929.40^{C}	$1367.55^{B\#}$	100.00^{A}	100.00^{A}	99.99^{C}	91.91^{D}	67.90^{D}
0.7	6.10^{E}	127.81^{E}	301.54^{D}	718.04^{D}	$1326.46^{C\#}$	100.00^{A}	100.00^{A}	99.99^{C}	99.99^{D}	91.39^{E}

* A, B, C, D, E, ' and # show statistic significant with 95 % confidence interval

APPENDIX D

Data of kinetic study and statistical analysis

Table D.1 One-way ANOVA of capacity between group CB-P and CB-M400 in kinetic study

			Sum of Squares	df	Mean Square	F	Sig.
Capacity	500 mg/L	Between Groups	105646.932	1	105646.932	1.290	.261
		Within Groups	4751672.405	58	81925.386		
		Total	4857319.337	59			
	100 mg/L	Between Groups	109719.650	1	109719.650	5.533	.022
		Within Groups	1150216.283	58	19831.315		
		Total	1259935.932	59			
Efficiency	500 mg/L	Between Groups	619.580	1	619.580	4.726	.034
		Within Groups	7603.098	58	131.088		
		Total	8222.678	59			
	100 mg/L	Between Groups	5826.701	1	5826.701	6.650	.012
		Within Groups	50822.203	58	876.245		
		Total	56648.904	59			

Table D.2 Pb (II) adsorption capacity (mg/g) of CB-P and CB-M400 in kinetic study with statistic significant between contact times

Time (Minute)	100 mg/L		Time (Minute)	500 mg/L	
	CB-P	CB-M400		CB-P	CB-M400
5	50.89^{A}	109.98^{A}	5	101.61^{A}	209.73^{A}
10	71.42^{A}	194.92^{B}	30	213.64^{B}	422.98^{B}
15	89.05^{A}	271.94^{C}	60	343.98^{C}	601.07^{C}
20	89.24^{A}	345.64^{D,}	90	561.82^{D}	755.84^{D}
30	160.76^{B}	416.65$^{E\#}$	120	717.92^{E}	786.68^{D,}
60	366.67^{C}	408.90$^{E\#}$	150	836.58^{F}	849.15^{E,}
120	403.69^{C}	408.86$^{E\#}$	180	849.66^{G}	869.07^{E,}
180	406.60^{C}	401.57$^{E\#}$	240	964.62^{H}	929.87$^{E\#}$
240	430.26^{C}	361.35^{E,}	300	960.66^{H}	958.16$^{F\#}$
360	436.15^{C}	440.19$^{\#}$	360	970.16^{H}	977.33^{F}

* ^{A}, ^{B}, ^{C}, ^{D} ^{E}, ^{F}, ^{G}, ^{H}, ‘ and $^{\#}$ show statistic significant with 95 % confidence interval

APPENDIX E

Data of interference study and statistical analysis

Table E.1 One-way ANOVA of Pb adsorption capacity between group CB-P and CB-M400 in single Pb, Pb+Cr and Pb+Fe system

		Sum of Squares	df	Mean Square	F	Sig.
Single Pb	Between Groups	6.184	1	6.184	2.888	.094
	Within Groups	137.026	64	2.141		
	Total	143.210	65			
Pb+Cr	Between Groups	.004	1	.004	.045	.833
	Within Groups	5.497	62	.089		
	Total	5.501	63			
Pb+Fe	Between Groups	2.961	1	2.961	2.373	.129
	Within Groups	77.349	62	1.248		
	Total	80.310	63			

Table E.2 Pb (II) adsorption capacity (mmol/g) of CB-P and CB-M400 in interference study with statistic significant between contact times of single Pb, Pb+Cr and Pb+Fe system

Time (Minute)	CB-P			CB-M400		
	Single Pb	Pb+Cr	Pb+Fe	Single Pb	Pb+Cr	Pb+Fe
15	0.39^{A}	0.23^{A}	0.90^{A}	1.35^{A}	0.47^{A}	1.24^{A}
30	0.95^{B}	0.32^{A}	1.73^{B}	2.21^{B}	0.40^{A}	1.94^{B}
45	1.64^{C}	0.28^{A}	2.20^{B,}	2.88^{C}	0.44^{A}	2.69^{C}
60	2.42^{D}	0.27^{A}	2.37^{C,}	3.41^{D}	0.37^{A}	2.77^{C,}
90	3.40^{E}	0.27^{A}	2.65$^{D,\#}$	4.04^{E}	0.41^{A}	3.76^{Da}
120	3.83^{E}	0.48^{A}	2.89$^{D\#}$	4.23E’	0.40^{A}	3.27$^{C,\#}$
180	3.88^{E}	0.56^{A}	3.00$^{D\#}$	4.41’	0.39^{A}	3.17$^{C,\#}$
240	3.90^{E}	0.56^{A}	2.81$^{D,\#}$	4.19^{E,}	0.45^{A}	3.47$^{D,\#}$
300	3.87^{E}	0.61^{A}	3.11$^{\#}$	4.19^{E,}	0.47^{A}	3.55^{Da}
360	3.89^{E}	0.67^{A}	2.97D$^{\#}$	3.99^{E}	0.34^{A}	4.05^{a}

* ^{A}, ^{B}, ^{C}, ^{D}, ^{E}, ‘, $^{\#}$, and ^{a} show statistic significant with 95 % confidence interval

APPENDIX F

Battery wastewater composition analysis, data of battery treatment study and statistical analysis

Table F.1 Wastewater quality and composition measurement procedure

Parameters	Measurement method
pH	Potentiometric
Total dissolved solid (TDS)	Gravimetric after filtration (Whatman GF/F)
Suspended solid (SS)	Gravimetric after filtration (Whatman GF/F)
Dissolved heavy metals	GF/F filtration and flame atomic absorption spectrophotometry
Particulate heavy metals	High performance microwave digestion (MILESTONE, ETHOS ONE) and flame atomic absorption spectrophotometry
NH_4^+	Phenate spectrophotometry
SO_4^{2-}	Nephelometry
Cl^-	Argentometric titration
PO_4^{3-}	Ascorbic acid spectrophotometry
NO_3^-	Cadmium reduction and spectrophotometry NO2

Table F.2 One-way ANOVA of wastewater quality after processed treatment I between group CB-P and CB-M400

		Sum of Squares	df	Mean Square	F	Sig.
pH	Between Groups	.009	1	.009	1.340	.259
	Within Groups	.145	22	.007		
	Total	.154	23			
TDS	Between Groups	.007	1	.007	.000	.989
	Within Groups	755.733	22	34.352		
	Total	755.740	23			
Pb	Between Groups	.091	1	.091	.368	.550
	Within Groups	5.444	22	.247		
	Total	5.535	23			
Cr	Between Groups	.002	1	.002	.231	.636
	Within Groups	.218	22	.010		
	Total	.220	23			
Ni	Between Groups	.008	1	.008	4.829	.039
	Within Groups	.035	22	.002		
	Total	.043	23			
Zn	Between Groups	.003	1	.003	2.685	.116
	Within Groups	.028	22	.001		
	Total	.032	23			
Mn	Between Groups	.009	1	.009	2.147	.157
	Within Groups	.090	22	.004		
	Total	.098	23			
Fe	Between Groups	.454	1	.454	.289	.596
	Within Groups	34.501	22	1.568		
	Total	34.955	23			

Table F.3 Data of wastewater quality after process treatment I with statistic significant between doses

Dose	CB-P							
	pH	TDS	Pb	Cr	Ni	Zn	Mn	Fe
0.2	1.28^{A}	34.70^{A}	1.87^{A}	1.90^{A}	0.86^{A}	0.80^{A}	1.01^{A}	90.27^{A}
1.0	1.30^{A}	33.50^{B}	1.91^{A}	1.82^{A}	0.85^{A}	0.79^{A}	0.98^{B}	89.95^{A}
2.0	1.34^{B}	32.10^{C}	1.58^{B}	1.79^{A}	0.85^{A}	0.78^{A}	0.91^{A}	89.15^{A}
10.0	1.47^{C}	21.37^{D}	0.72^{C}	1.87^{A}	0.88^{A}	0.84^{B}	1.00^{A}	88.37^{A}
Dose	CB-M400							
	pH	TDS	Pb	Cr	Ni	Zn	Mn	Fe
0.2	1.33^{A}	35.50^{A}	1.78^{A}	1.83^{A}	0.86^{A}	0.77^{A}	1.00^{A}	89.77^{A}
1.0	1.38^{A}	33.70^{B}	1.74^{A}	1.81^{A}	0.82^{A}	0.76^{A}	0.95^{A}	89.22^{A}
2.0	1.33^{A}	31.93^{C}	1.42^{B}	1.76^{A}	0.80^{A}	0.75^{A}	0.88^{A}	89.77^{A}
10.0	1.50^{B}	20.40^{D}	0.63^{C}	1.91^{A}	0.82^{A}	0.84^{B}	0.92^{A}	90.08^{A}

* ^{A}, ^{B}, ^{C} and ^{D} show statistic significant with 95 % confidence interval

Table F.4 One-way ANOVA of wastewater quality after processed treatment II between group CB-P and CB-M400

		Sum of Squares	df	Mean Square	F	Sig.
pH	Between Groups	.381	1	.381	.564	.459
	Within Groups	18.910	28	.675		
	Total	19.291	29			
TDS	Between Groups	.015	1	.015	11.223	.002
	Within Groups	.038	28	.001		
	Total	.054	29			
Pb	Between Groups	.033	1	.033	2.748	.109
	Within Groups	.339	28	.012		
	Total	.372	29			
Cr	Between Groups	.001	1	.001	1.336	.258
	Within Groups	.011	28	.000		
	Total	.011	29			
Ni	Between Groups	.016	1	.016	.168	.685
	Within Groups	2.747	28	.098		
	Total	2.764	29			
Zn	Between Groups	.007	1	.007	.176	.678
	Within Groups	1.191	28	.043		
	Total	1.199	29			
Mn	Between Groups	.023	1	.023	1.128	.297
	Within Groups	.583	28	.021		
	Total	.606	29			
Fe	Between Groups	1.251	1	1.251	1.986	.170
	Within Groups	17.644	28	.630		
	Total	18.895	29			

Table F.5 Data of wastewater quality after process treatment II with statistic significant between doses

Dose	CB-P							
	pH	TDS	Pb	Cr	Ni	Zn	Mn	Fe
0.2	5.41^{A}	13.72^{A}	0.34^{A}	0.25^{A}	0.97^{A}	0.57^{A}	0.91^{A}	2.61^{A}
0.4	7.45^{B}	13.78’	0.00^{B}	0.25^{A}	0.27^{B}	0.00^{B}	0.64^{B}	0.01^{A}
0.6	8.00^{C}	$13.76^{A,}$	0.00^{B}	0.25^{A}	0.17^{C}	0.00^{B}	0.53^{C}	0.00^{A}
0.8	$8.14^{D,}$	$13.76^{A,}$	0.00^{B}	0.25^{A}	0.17^{C}	0.00^{B}	0.52^{C}	0.00^{A}
1.0	8.21’	$13.75^{A,}$	0.00^{B}	0.25^{A}	0.16^{C}	0.00^{B}	0.51^{C}	0.00^{A}
Dose	CB-M400							
	pH	TDS	Pb	Cr	Ni	Zn	Mn	Fe
0.2	7.07^{A}	13.74^{A}	0.01^{A}	0.24^{A}	0.97^{A}	0.41^{A}	0.91^{A}	0.57^{A}
0.4	7.45^{B}	$13.78^{A,}$	0.00^{A}	0.24^{A}	0.34^{B}	0.00^{B}	0.69^{B}	0.00^{A}
0.6	7.84^{C}	$13.81^{B,}$	0.00^{A}	0.25^{A}	0.24^{C}	0.00^{B}	0.61^{C}	0.00^{A}
0.8	7.96^{C}	$13.84^{B,}$	0.00^{A}	0.24^{A}	0.21^{C}	0.00^{B}	0.60^{C}	0.00^{A}
1.0	8.01^{C}	$13.82^{B,}$	0.00^{A}	0.24^{A}	0.21^{C}	0.00^{B}	0.58^{C}	0.00^{A}

* ^{A}, ^{B}, ^{C} and ^{D} show statistic significant with 95 % confidence interval

Table F.6 One-way ANOVA of wastewater quality after processed treatment III between group CB-P, CB-M400, $CaCO_3$ and $Ca(OH)_2$

		Sum of Squares	df	Mean Square	F	Sig.
pH	Between Groups	14.480	3	4.827	1.758	.166
	Within Groups	153.741	56	2.745		
	Total	168.221	59			
TDS	Between Groups	.480	3	.160	3.476	.022
	Within Groups	2.578	56	.046		
	Total	3.058	59			
Pb	Between Groups	.243	3	.081	1.217	.312
	Within Groups	3.724	56	.067		
	Total	3.967	59			
Cr	Between Groups	4.904	3	1.635	2.336	.084
	Within Groups	39.191	56	.700		
	Total	44.095	59			
Ni	Between Groups	.544	3	.181	4.642	.006
	Within Groups	2.189	56	.039		
	Total	2.733	59			
Zn	Between Groups	.200	3	.067	1.001	.399
	Within Groups	3.723	56	.066		
	Total	3.923	59			
Mn	Between Groups	1.386	3	.462	5.156	.003
	Within Groups	5.017	56	.090		
	Total	6.402	59			
Fe	Between Groups	8638.222	3	2879.407	2.245	.093
	Within Groups	71821.089	56	1282.519		
	Total	80459.311	59			

Table F.7 Data of wastewater quality after process treatment III with statistic significant between doses

Dose	CB-P							
	pH	TDS	Pb	Cr	Ni	Zn	Mn	Fe
0.2	2.47^{A}	3.30^{A}	0.68^{A}	2.09^{A}	0.88^{A}	0.85^{A}	1.38^{A}	92.20^{A}
0.4	2.66^{B}	3.12^{B}	0.66^{A}	2.06^{A}	0.89^{A}	0.74^{A}	1.37^{A}	91.09^{A}
0.6	2.92^{C}	2.97^{C}	0.60^{B}	2.03^{A}	0.89^{A}	0.70^{A}	1.40^{A}	84.07^{B}
0.8	3.25^{D}	2.84^{D}	0.49^{C}	1.64^{B}	0.88^{A}	0.77^{A}	1.37^{A}	44.37^{C}
1.0	5.59^{E}	2.66^{E}	0.02^{D}	0.09^{C}	0.74^{B}	0.33^{B}	1.28^{A}	6.11^{D}
Dose	CB-M400							
	pH	TDS	Pb	Cr	Ni	Zn	Mn	Fe
0.2	2.40^{A}	3.37^{A}	0.61^{A}	2.05^{A}	0.86^{A}	0.83^{A}	1.38^{A}	84.83^{A}
0.4	2.60^{B}	3.19^{B}	0.60^{A}	2.03^{A}	0.86^{A}	0.75^{A}	1.38^{A}	92.31^{A}
0.6	2.92^{C}	2.95^{C}	0.55^{B}	2.03^{A}	0.85^{A}	0.74^{A}	1.35^{A}	85.54^{A}
0.8	3.38^{D}	2.80^{D}	0.44^{C}	1.63^{B}	0.85^{A}	0.82^{A}	1.32^{A}	43.86^{B}
1.0	5.90^{E}	2.67^{E}	0.01^{D}	0.08^{C}	0.68^{B}	0.25^{B}	1.20^{B}	2.56^{C}
Dose	$CaCO_3$							
	pH	TDS	Pb	Cr	Ni	Zn	Mn	Fe
0.2	2.83^{A}	3.00^{A}	0.71^{A}	2.06^{A}	0.91^{A}	0.74^{A}	1.34^{A}	85.47^{A}
0.4	3.20^{A}	2.84^{B}	0.51^{B}	1.78^{B}	0.91^{A}	0.78^{A}	1.36^{A}	50.85^{B}
0.6	4.11^{B}	2.72^{C}	0.35^{C}	0.47^{C}	0.85^{A}	0.68^{A}	1.33^{A}	21.99^{C}
0.8	5.25^{C}	2.68^{C},	0.03^{D}	0.11^{D}	0.80^{A}	0.40^{B}	1.17^{A}	10.32^{D}
1.0	6.22^{D}	2.65’	0.00^{D}	0.10^{D}	0.48^{B}	0.13^{C}	0.75^{B}	3.13^{E}
Dose	$Ca(OH)_2$							
	pH	TDS	Pb	Cr	Ni	Zn	Mn	Fe
0.2	2.63^{A}	3.19^{A}	0.69^{A}	2.02^{A}	0.82^{A}	0.79^{A}	1.30^{A}	92.02^{A}
0.4	2.86^{A},	2.97^{B}	0.63^{A}	1.98^{A}	0.80^{A},	0.74^{A}	1.29^{A}	89.52^{A}
0.6	3.26’	2.79^{C}	0.43^{B}	1.52^{B}	0.75’	0.74^{A}	1.23^{A},	37.78^{B}
0.8	4.48^{B}	2.71^{D}	0.25^{C}	0.18^{C}	0.67^{B}	0.68^{B}	1.04’	10.97^{C}
1.0	9.03^{C}	2.64^{E}	0.02^{D}	0.09^{C}	0.00^{C}	0.00^{C}	0.00^{B}	0.03^{D}

* ^{A}, ^{B}, ^{C}, ^{D}, ^{E} and ‘ show statistic significant with 95 % confidence interval

VITA

Mr. Pathompong Vibhatabandhu was born on January 31, 1992 in Bangkok, Thailand. He participated in poster presentation of the Science Forum 2014 at Chulalongkorn University, Bangkok, Thailand with the topic “Removal of copper (II) from synthetic wastewater using cuttlebone” and received Bachelor’s degree of Science, majoring environmental science from Chulalongkorn University in 2014. He has pursued Master’s degree in Biotechnology since 2014 and finished his study in 2016.